Supporting Information for "Seismic structure of the St. Paul Fracture Zone and Late Cretaceous to Mid Eocene oceanic crust in the equatorial Atlantic Ocean near 18°W"

Kevin Growe[1,2], Ingo Grevemeyer[1], Satish Singh[2], Milena Marjanović[2], Emma P. M. Gregory[2], Cord Papenberg[1], Venkata Vaddineni[2], Laura Gómez de la Peña[1], and Zhikai Wang[2]

[1]GEOMAR Helmholz Centre for Ocean Research Kiel

[2]Université de Paris, Institut de Physique du Globe de Paris; CNRS, Paris, France

Contents of this file

1. Figures S1 to S15
2. Tables S1 to S3

Introduction

Table S1 lists the acquisition parameters of the two seismic refraction lines used for this study. Figures S1a-S1n and S2a-S2o show all OBS record sections with corresponding traveltime fits and raypaths, for both lines, LI-02 and IS-01, respectively. Figures S3 and S4 illustrate the OBS mirrow image and the post-stack time-migrated MCS sections, that were used to constrain the basement depth below the seafloor for line LI-02 and IS-01,

respectively. Figure S5 depicts the porosity-velocity-aspect-ratio dependencies computed with a differential effective medium analysis after Taylor and Singh (2002). Figures S6-S15 show the results of several resolution tests for the tomographic inversion: 1. crustal checkerboard tests, 2. Moho regularization tests 3. Moho resolution tests and 4. mantle resolution tests. Their results and implications are briefly discussed in the main text. Table S2 lists all discretization, forward and inversion parametrization used for this study. And finally, Table S3 compares the different parametrization for the PmP inversion.

Table S1. Refraction line acquisition parameters.

Parameter/Line	**LI-02**	**IS-01**
Profile length [km]	143	350
Number of OBS	14	15
Mean OBS-spacing [km]	8.6	14.2
Number of shots	875	1167
Shot spacing [km]	∼0.16	0.3
Sampling frequency [Hz]	250	250
Total airgun volume [l]	86	82
Airgun array towing depth [m]	7.5	10

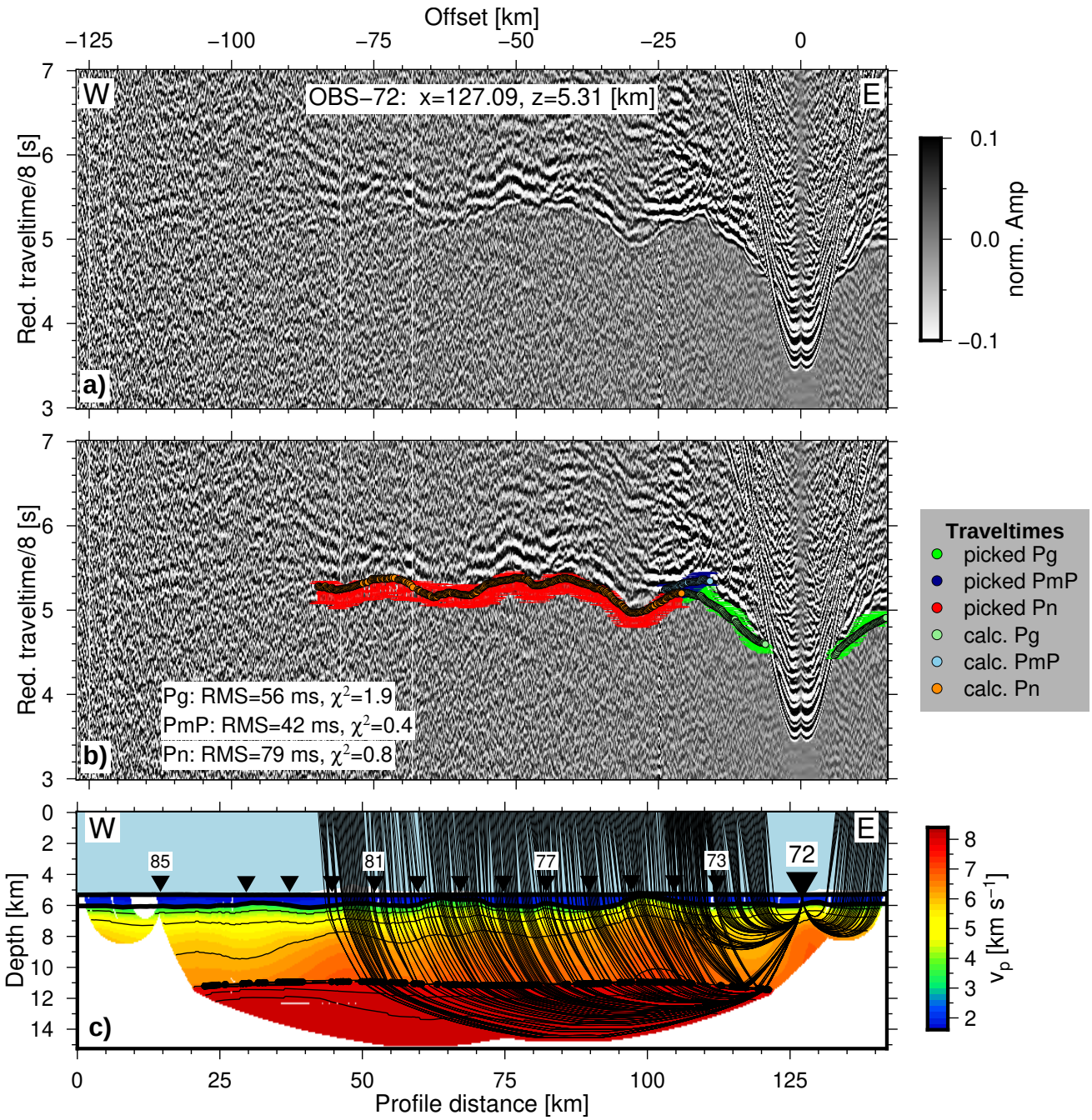

Figure S1a. **(a)** Record section of OBS 72 (LI-02) with **(b)** superimposed picked (small dots with error bars, indicating pick uncertainty) and computed traveltimes (larger dots). The time is reduced with a reduction velocity of 8 km/s. The amplitude is normalized and clipped to 10 %. **(c)** Corresponding raypaths superimposed on final velocity model. The velocity contour interval is 1.0 km/s for the crust, starting with 4 km/s, and 0.1 km/s for the mantle, starting at 8.0 km/s. Remaining figure elements are the same as in Fig. 4 in the main text.

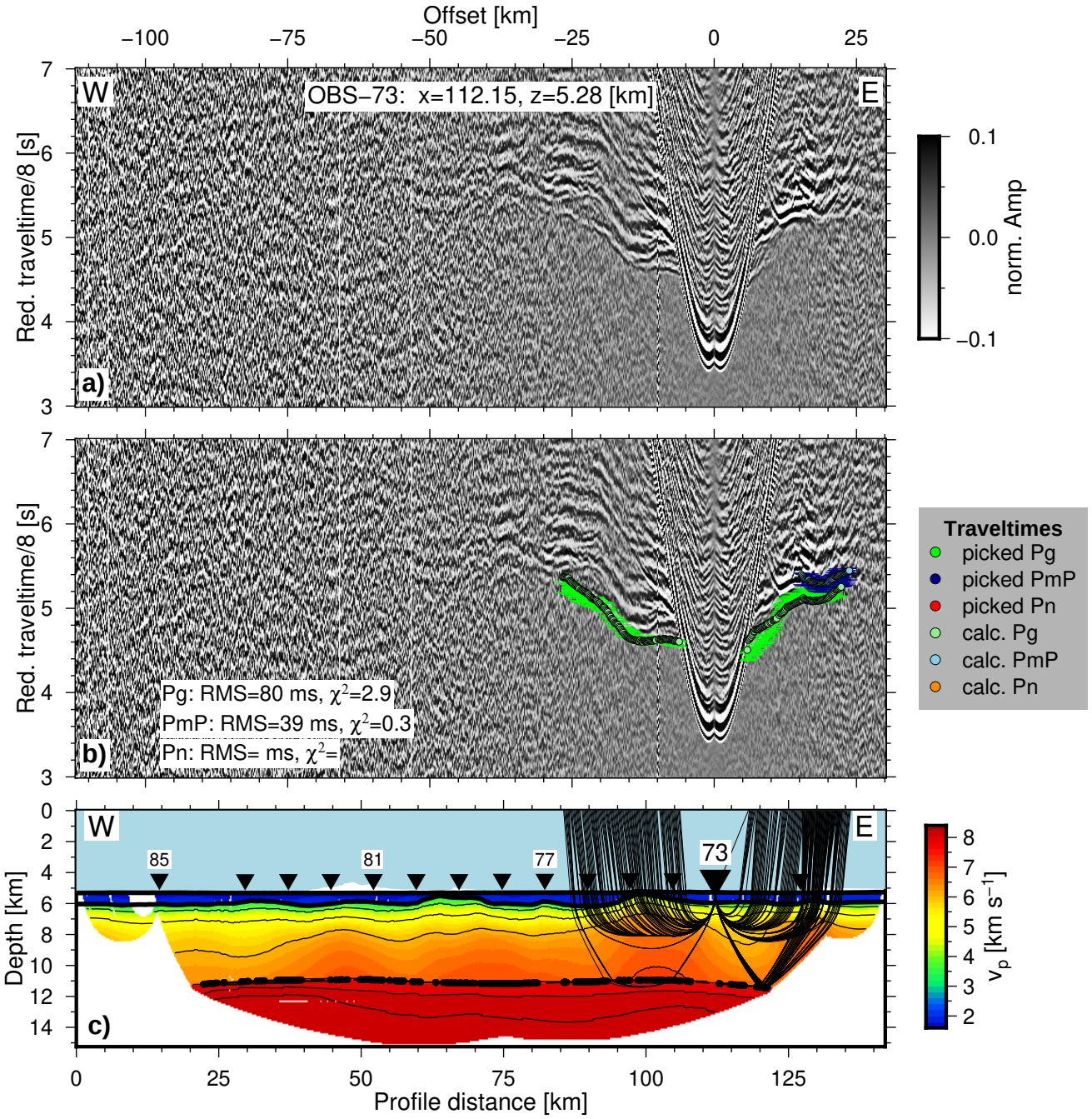

Figure S1b. Record section, traveltime fit and raypaths for OBS 73 (LI-02).

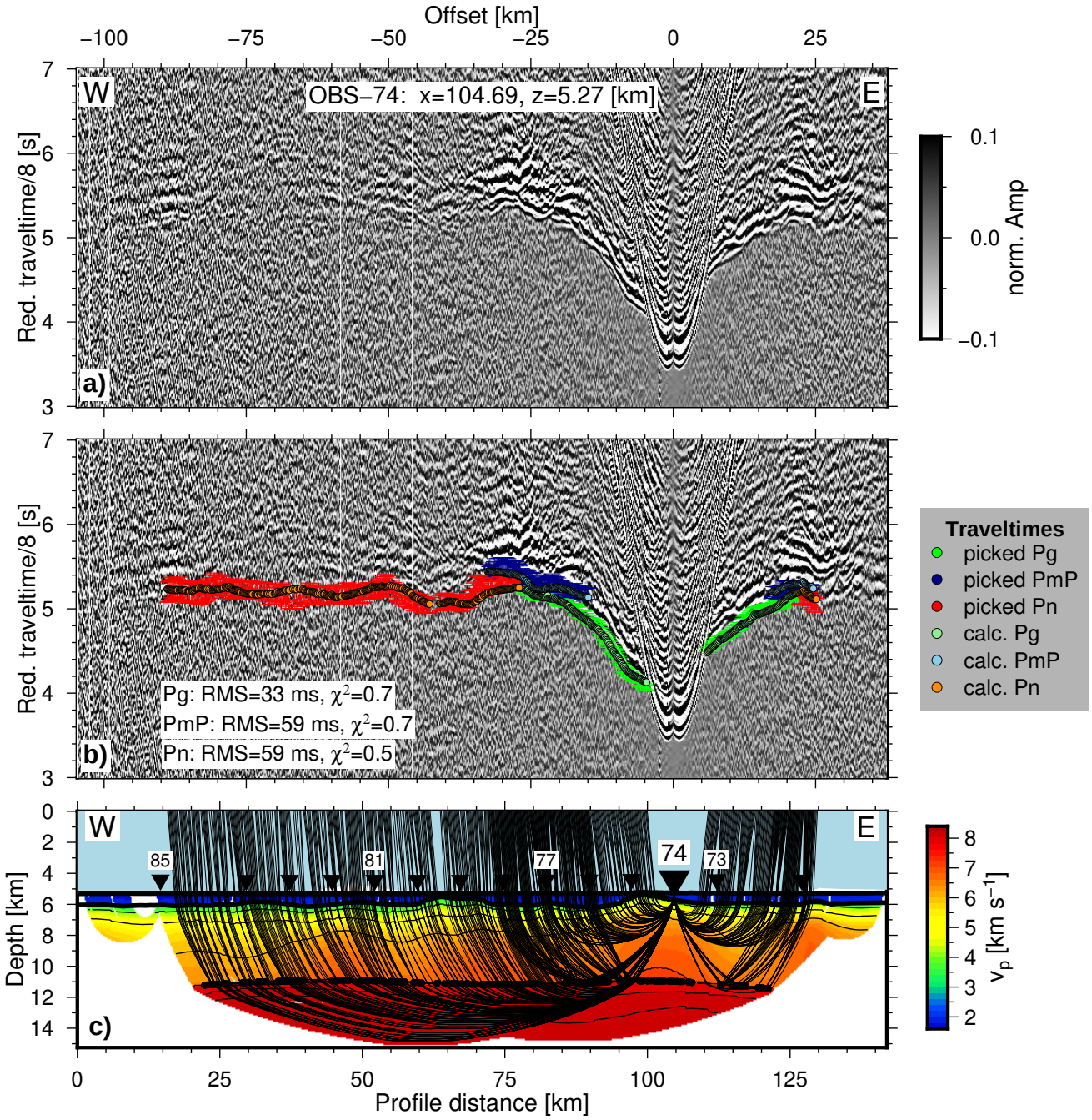

Figure S1c. Record section, traveltime fit and raypaths for OBS 74 (LI-02).

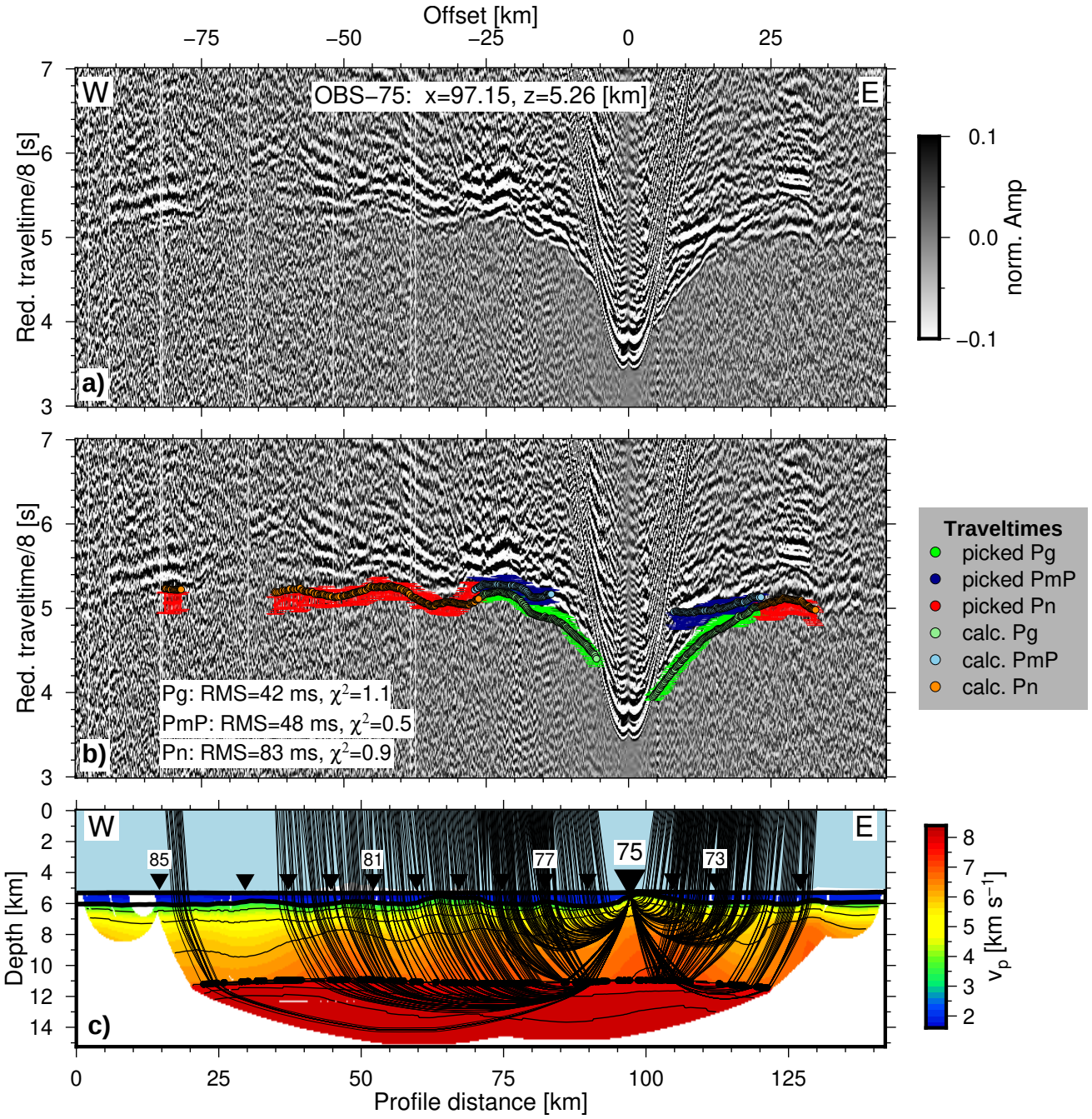

Figure S1d. Record section, traveltime fit and raypaths for OBS 75 (LI-02).

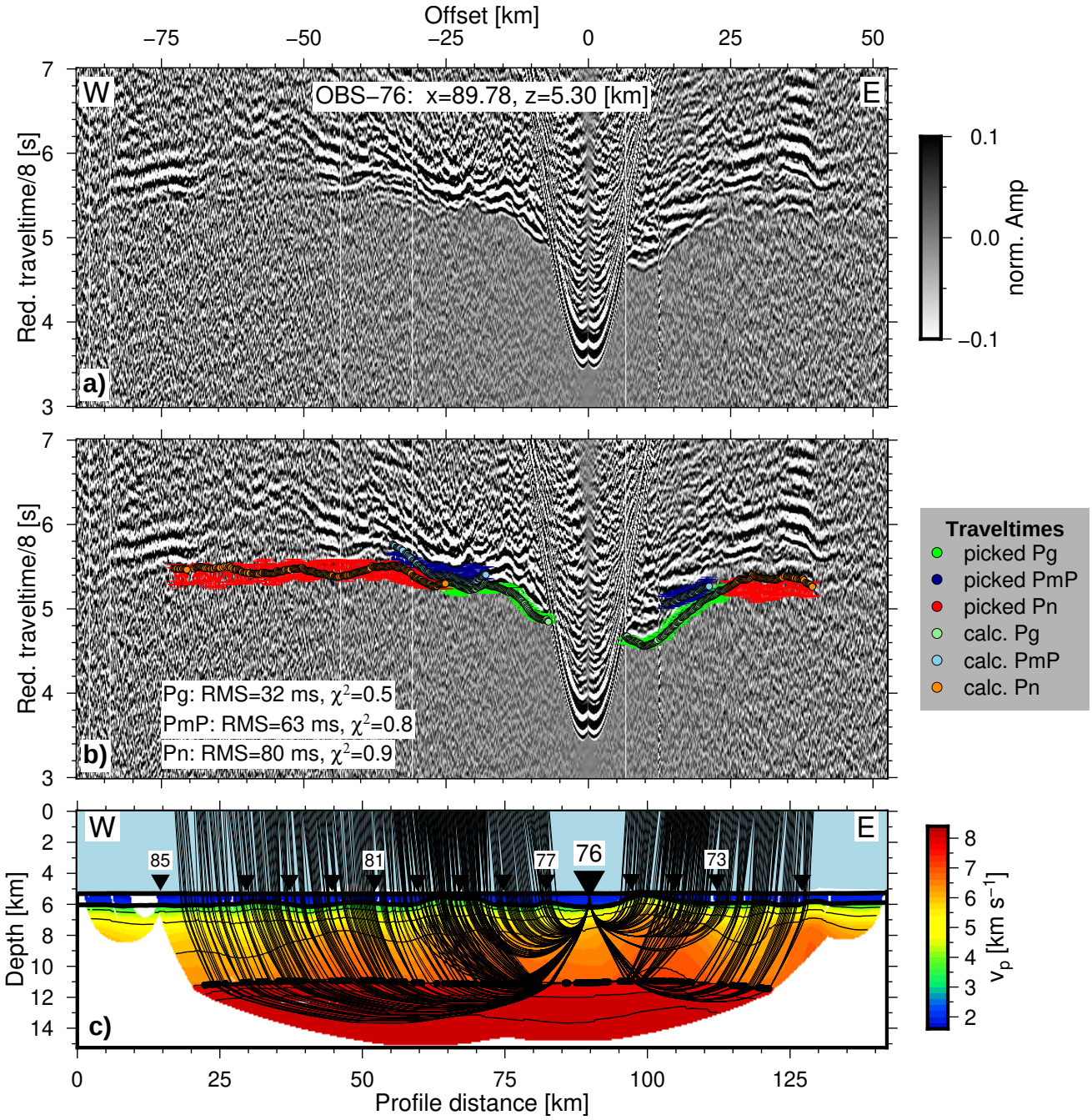

Figure S1e. Record section, traveltime fit and raypaths for OBS 76 (LI-02).

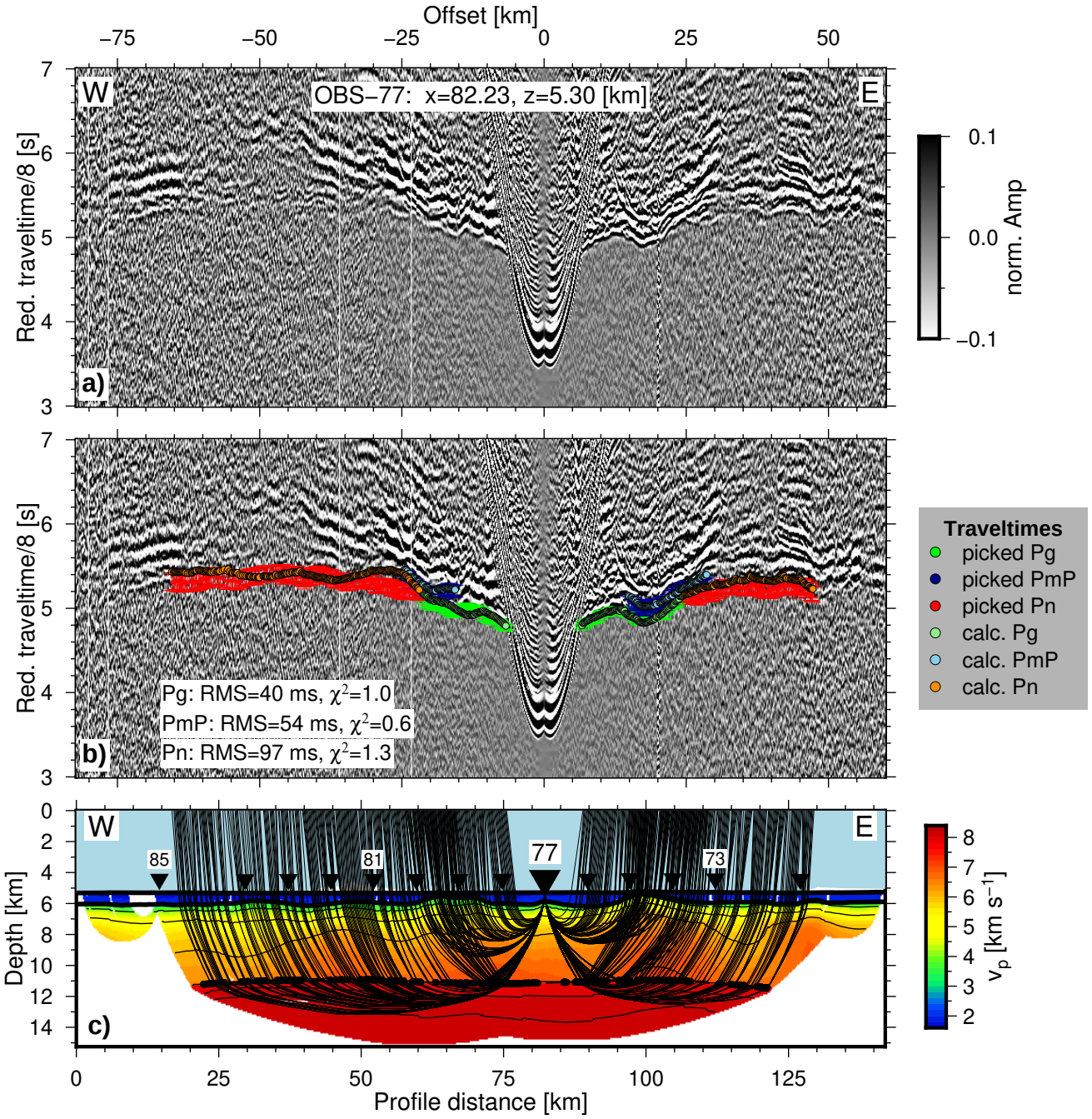

Figure S1f. Record section, traveltime fit and raypaths for OBS 77 (LI-02).

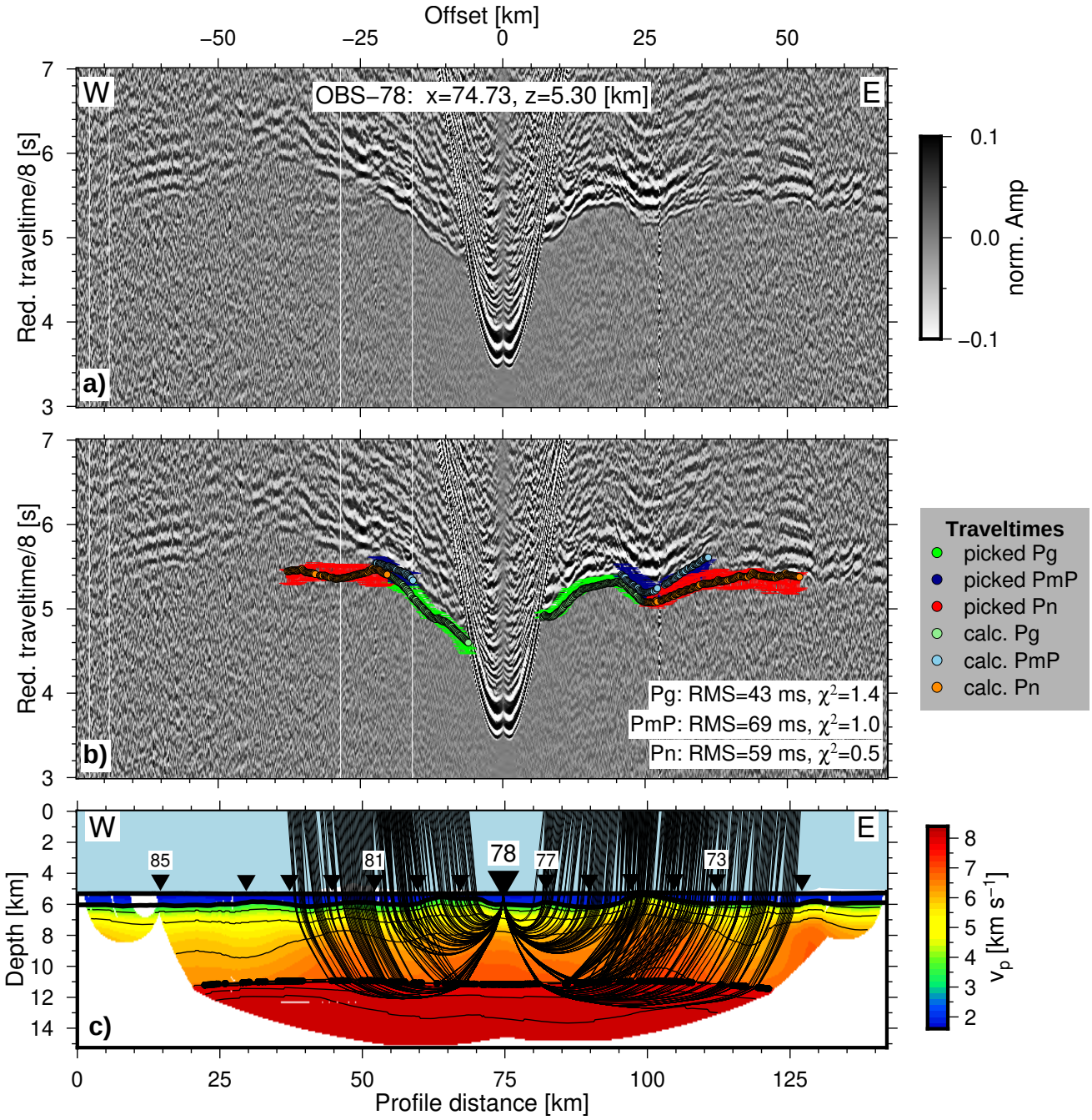

Figure S1g. Record section, traveltime fit and raypaths for OBS 78 (LI-02).

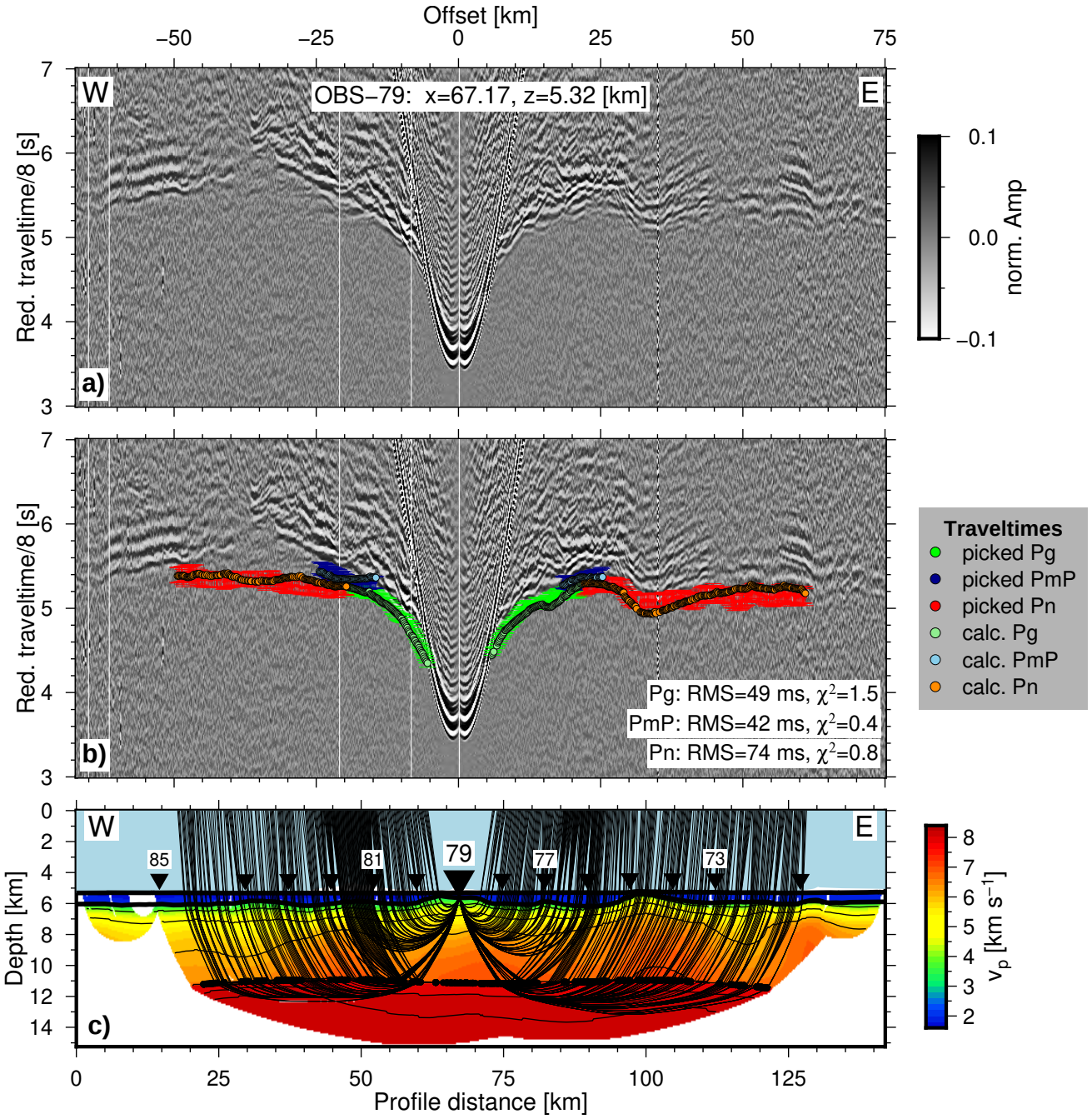

Figure S1h. Record section, traveltime fit and raypaths for OBS 79 (LI-02).

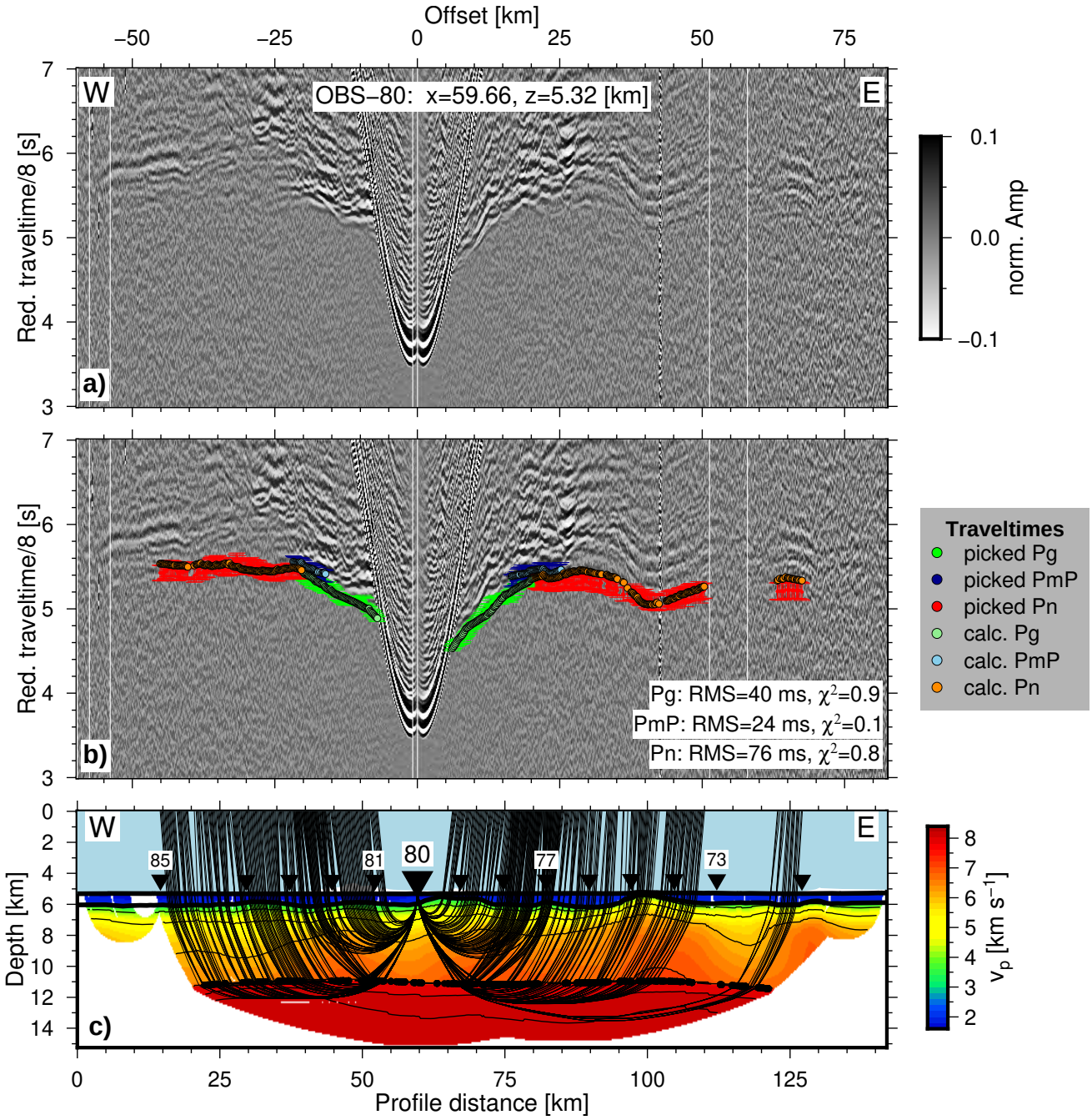

Figure S1i. Record section, traveltime fit and raypaths for OBS 80 (LI-02).

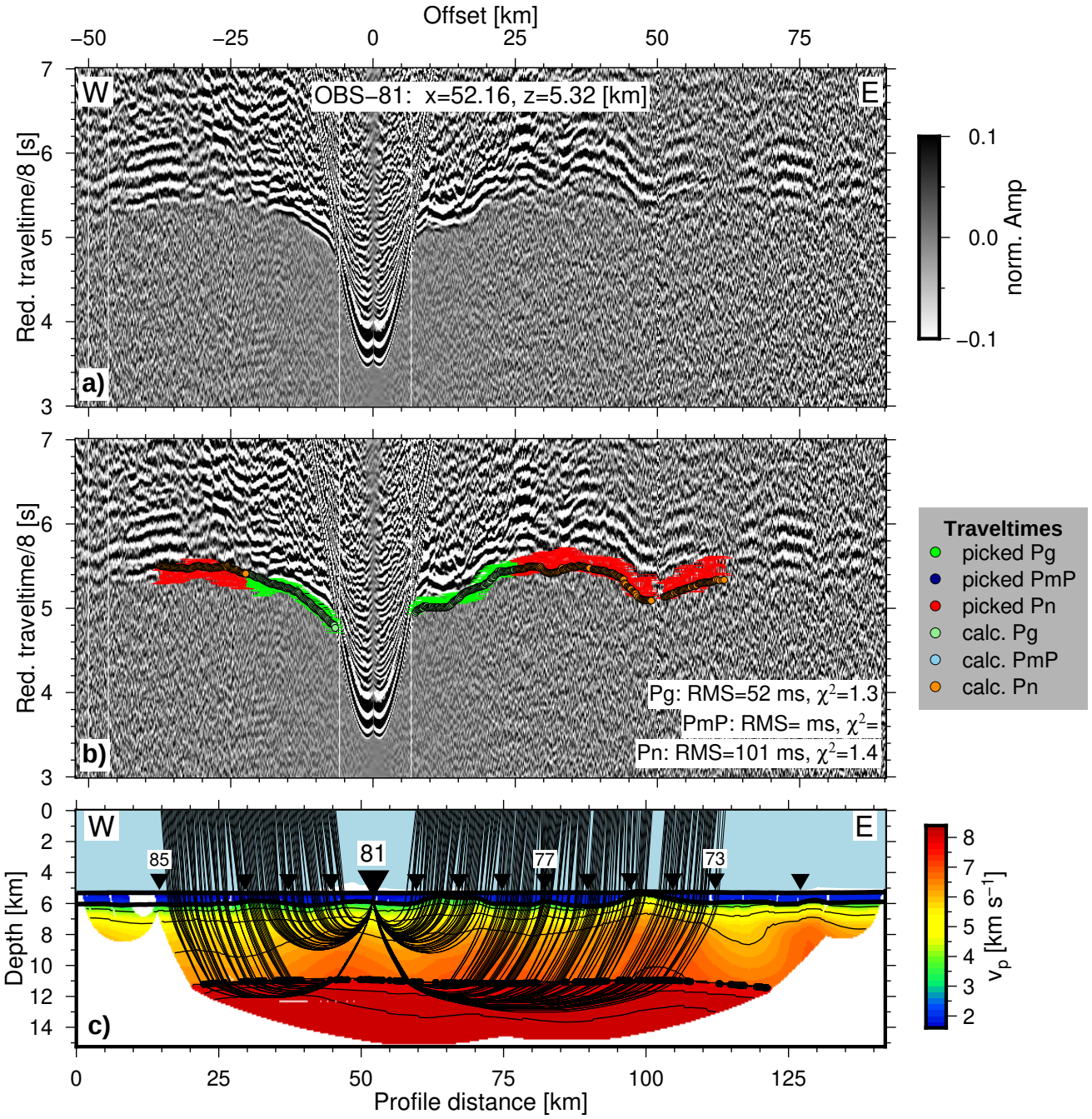

Figure S1j. Record section, traveltime fit and raypaths for OBS 81 (LI-02).

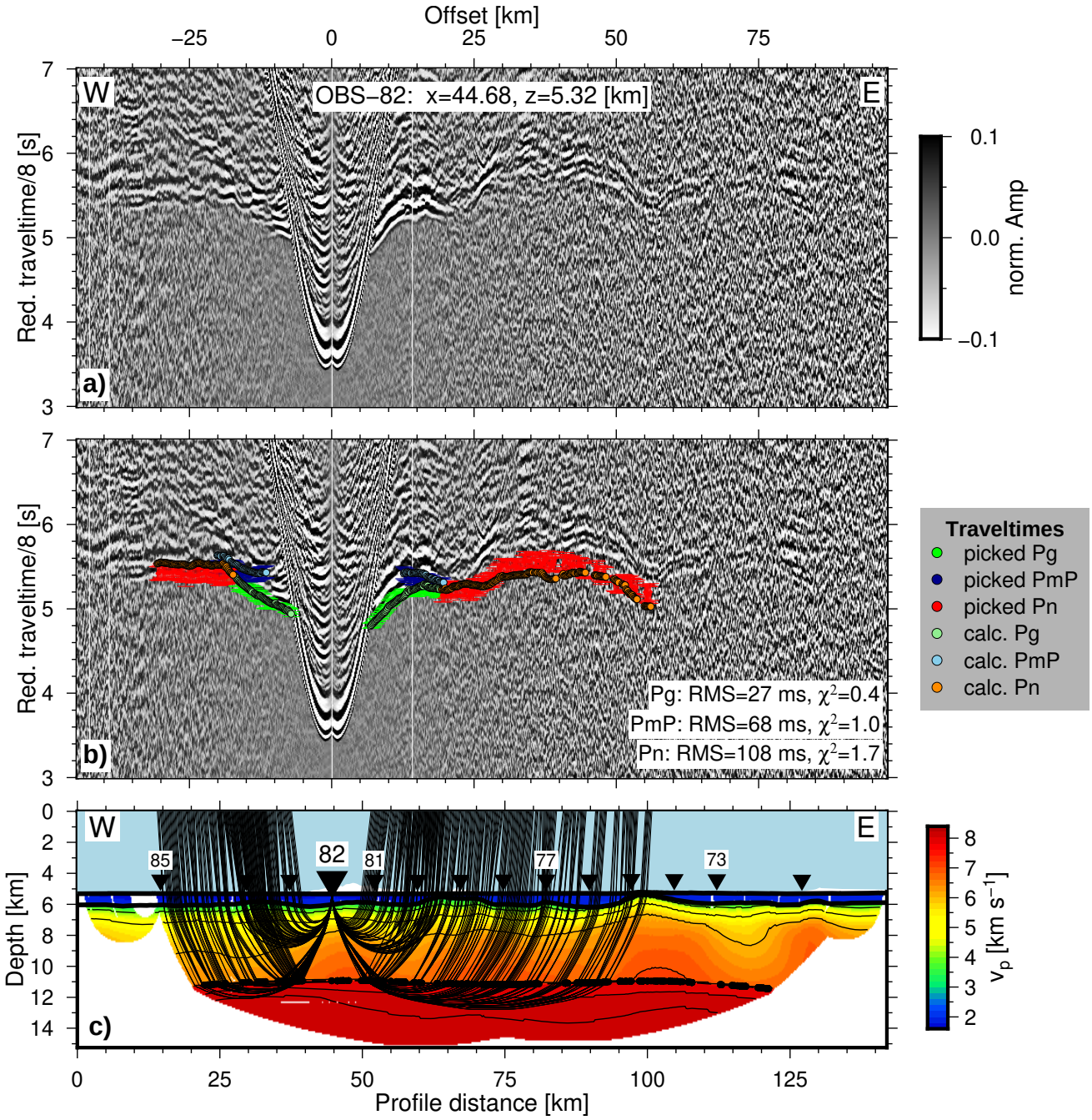

Figure S1k. Record section, traveltime fit and raypaths for OBS 82 (LI-02) .

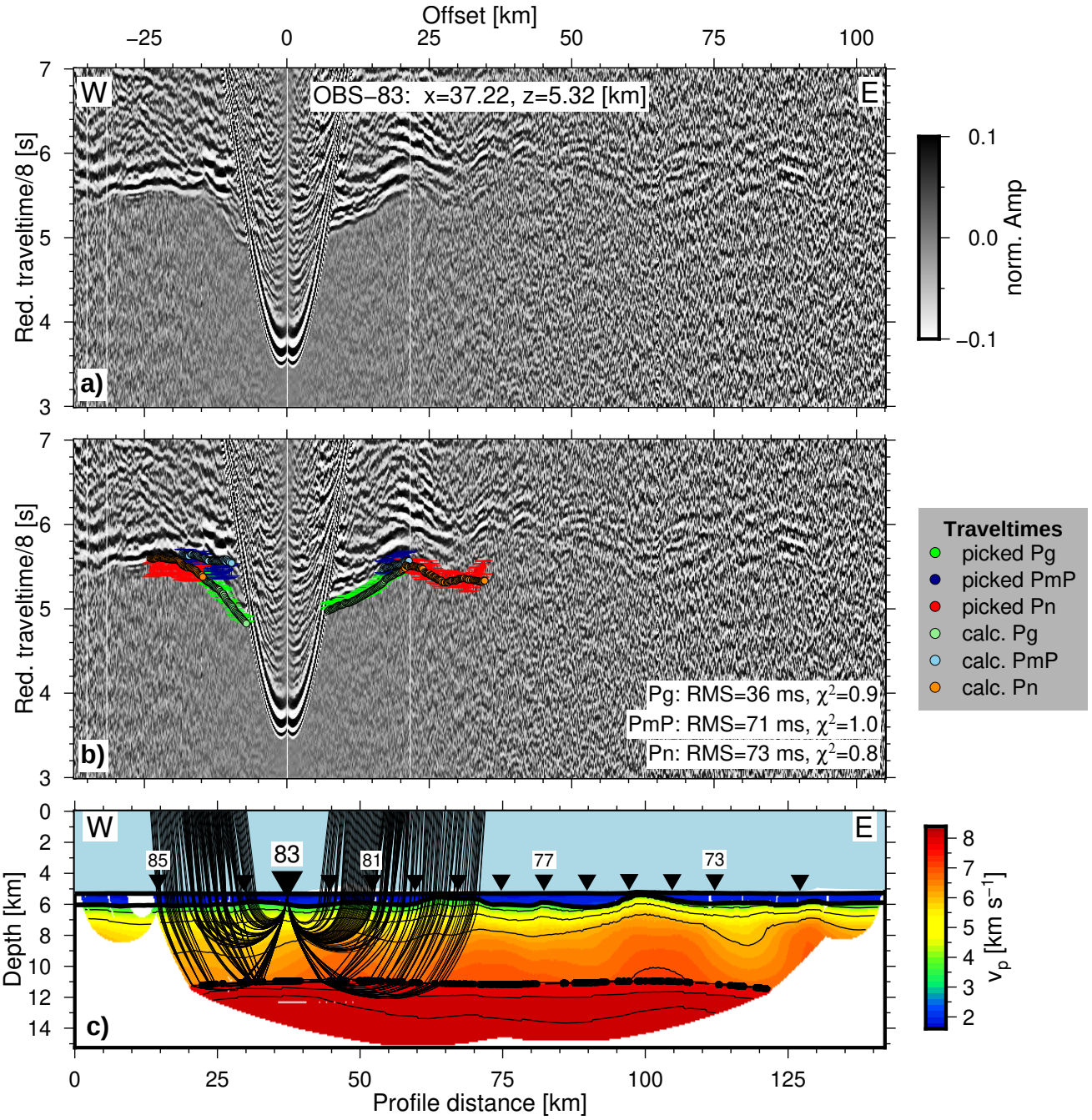

Figure S1l. Record section, traveltime fit and raypaths for OBS 83 (LI-02).

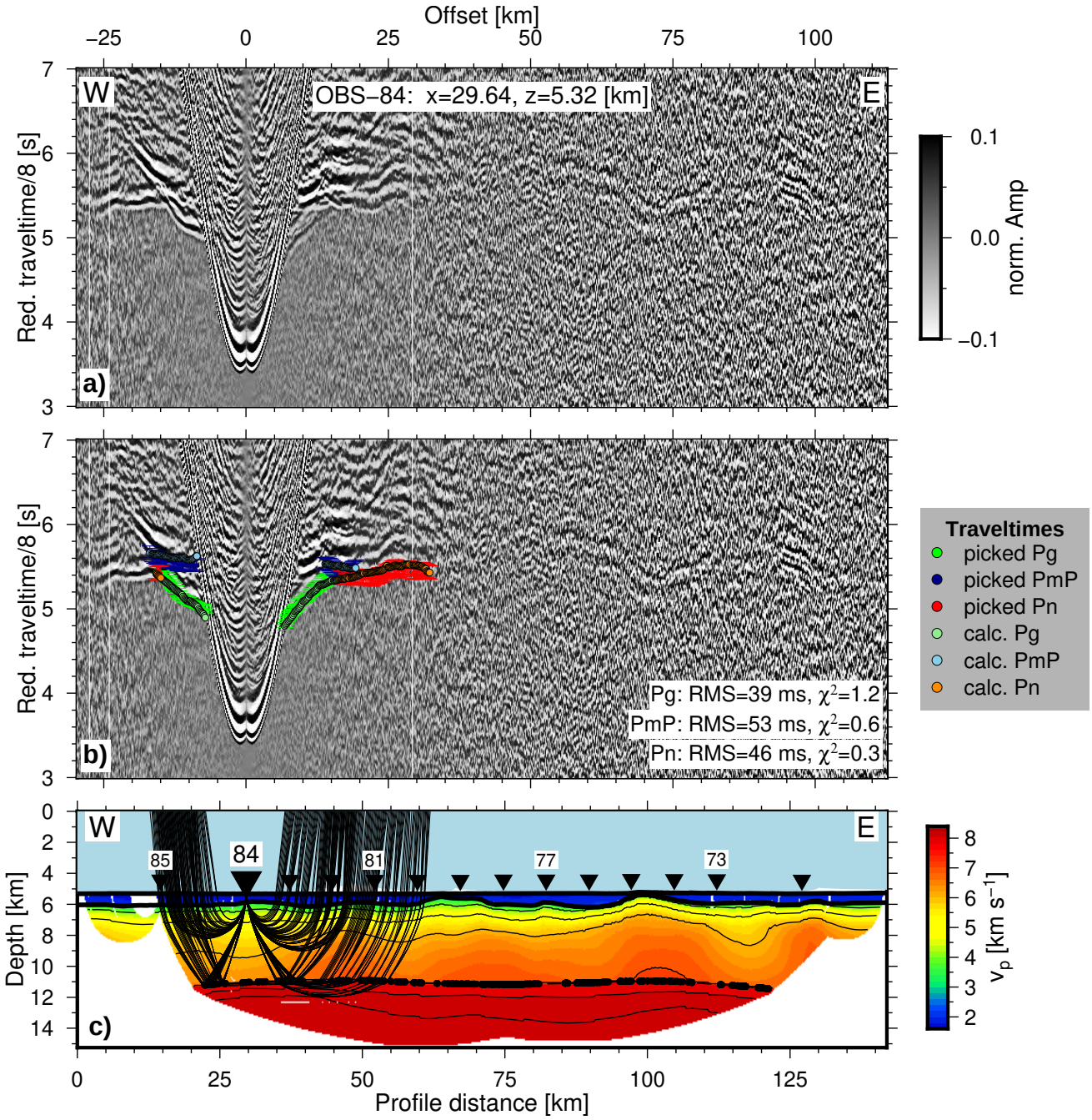

Figure S1m. Record section, traveltime fit and raypaths for OBS 84 (LI-02).

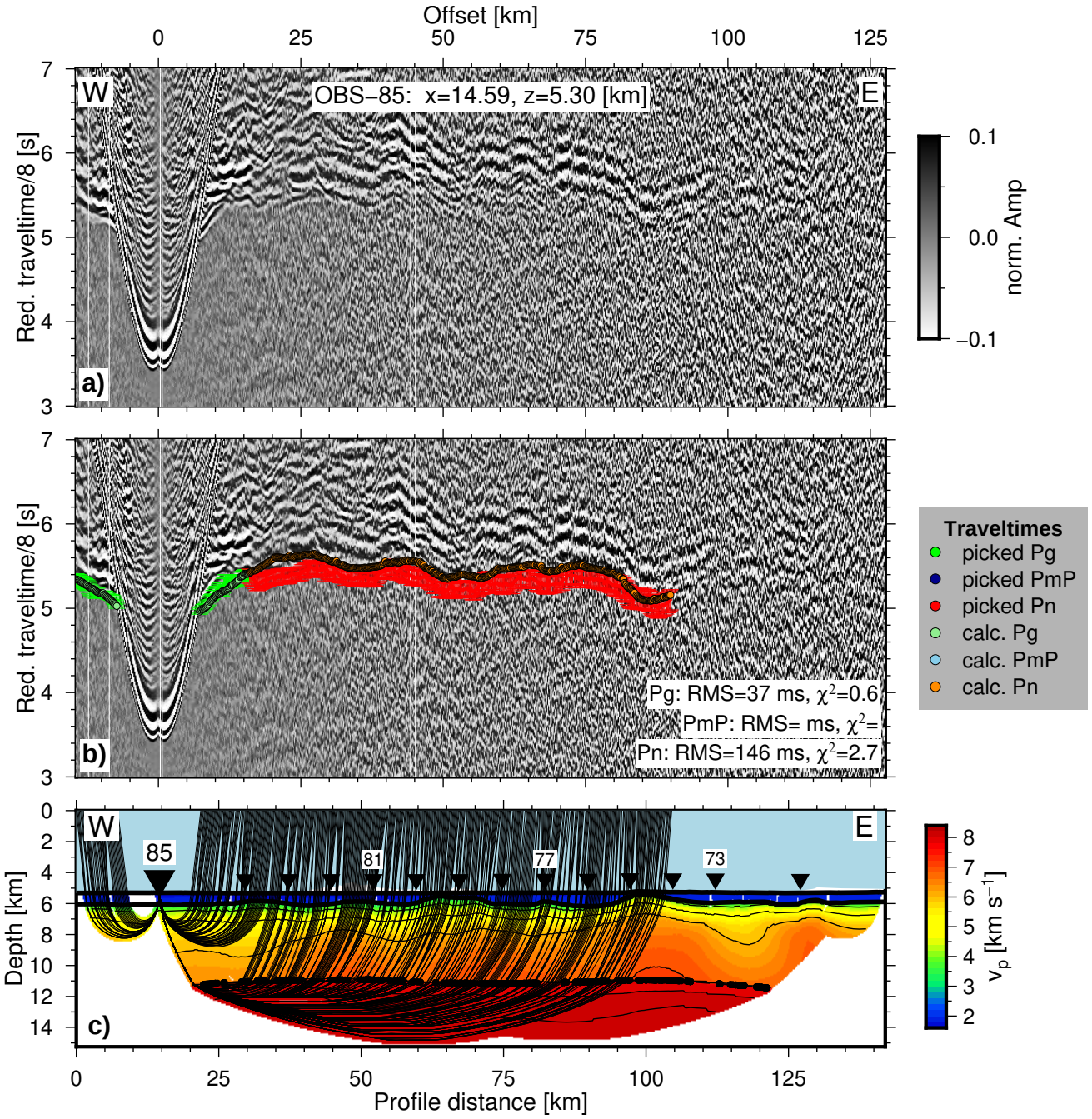

Figure S1n. Record section, traveltime fit and raypaths for OBS 85 (LI-02).

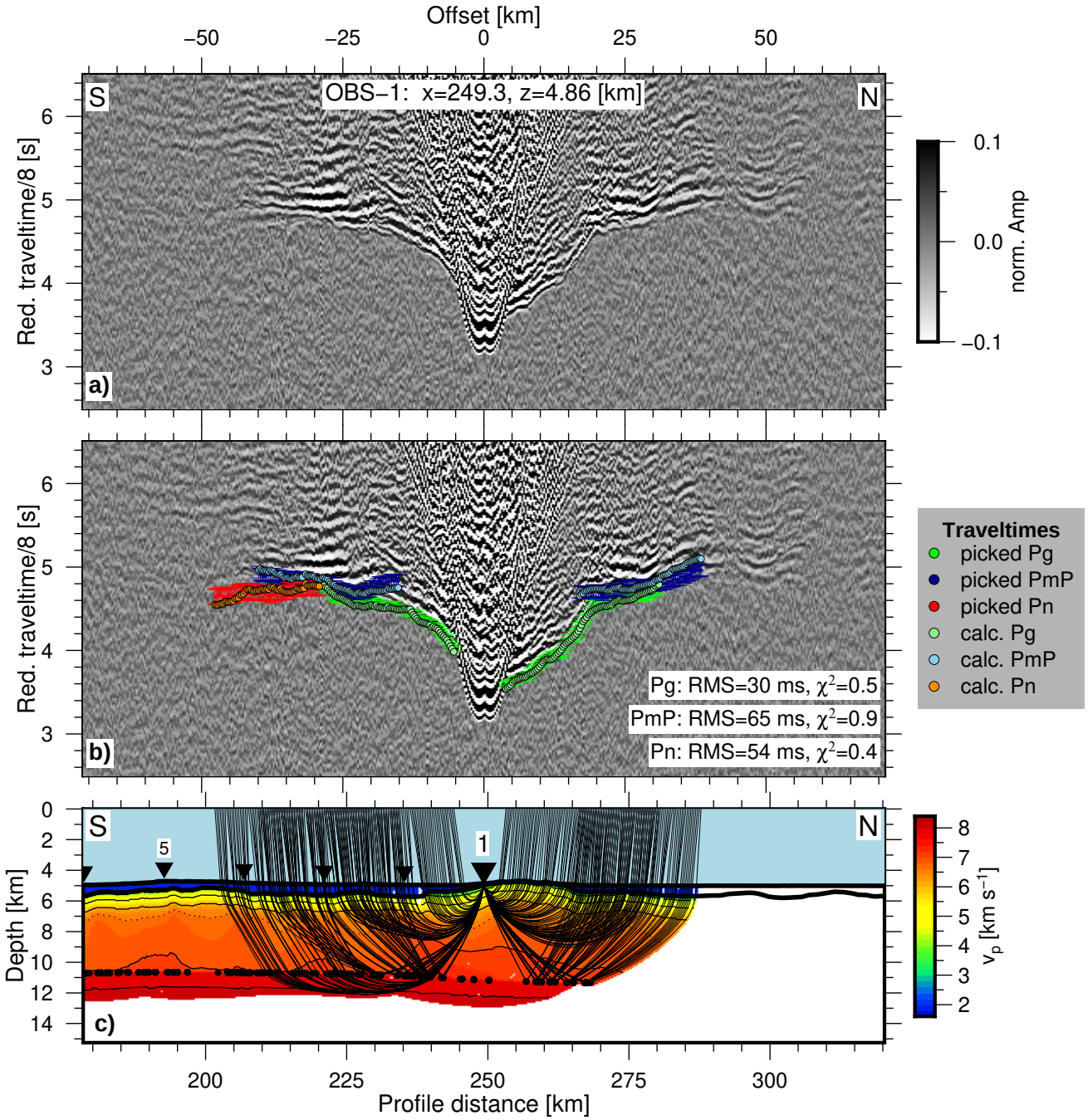

Figure S2a. Record section, traveltime fit and raypaths for OBS 01 (IS-01).

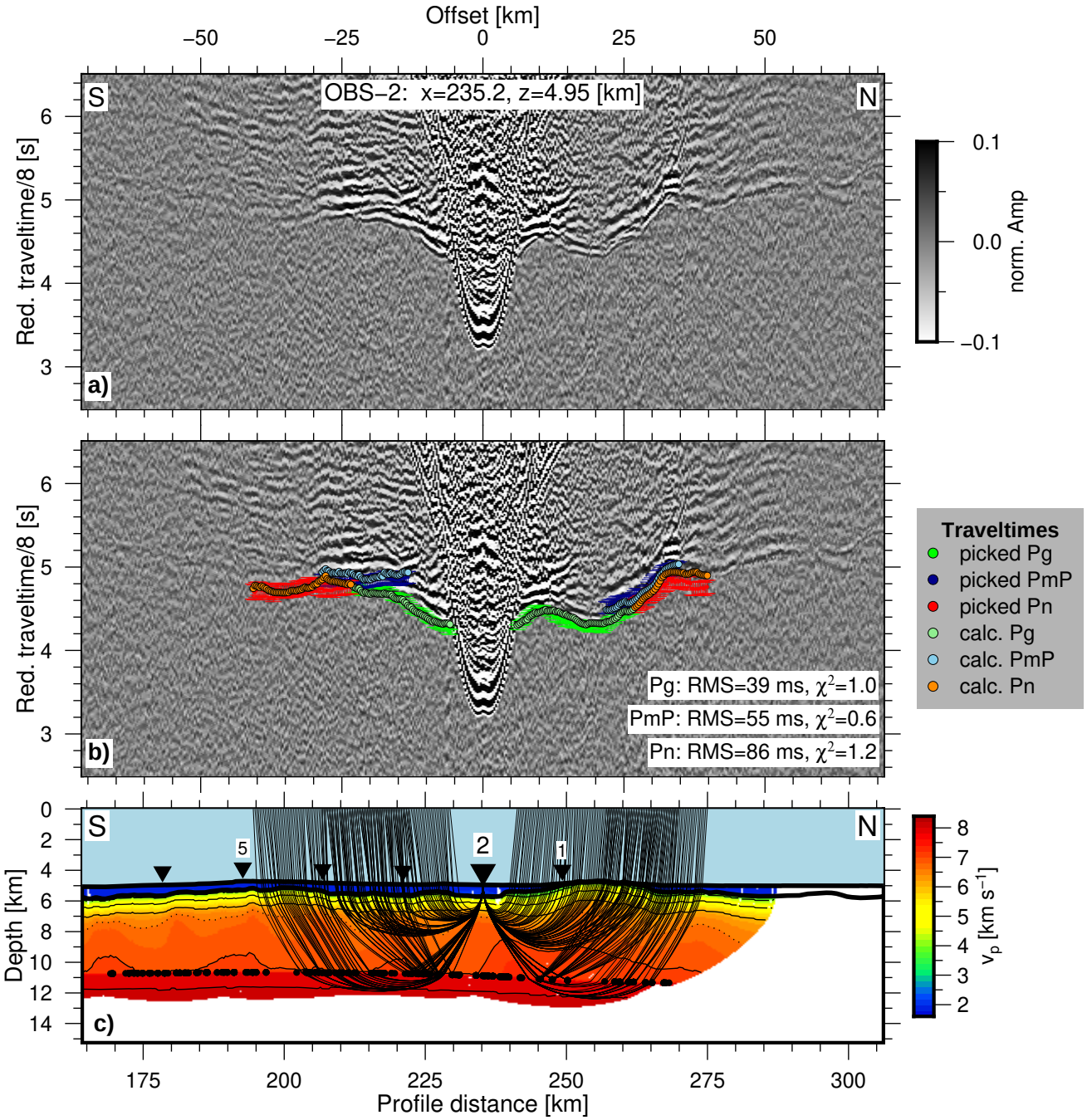

Figure S2b. Record section, traveltime fit and raypaths for OBS 02 (IS-01).

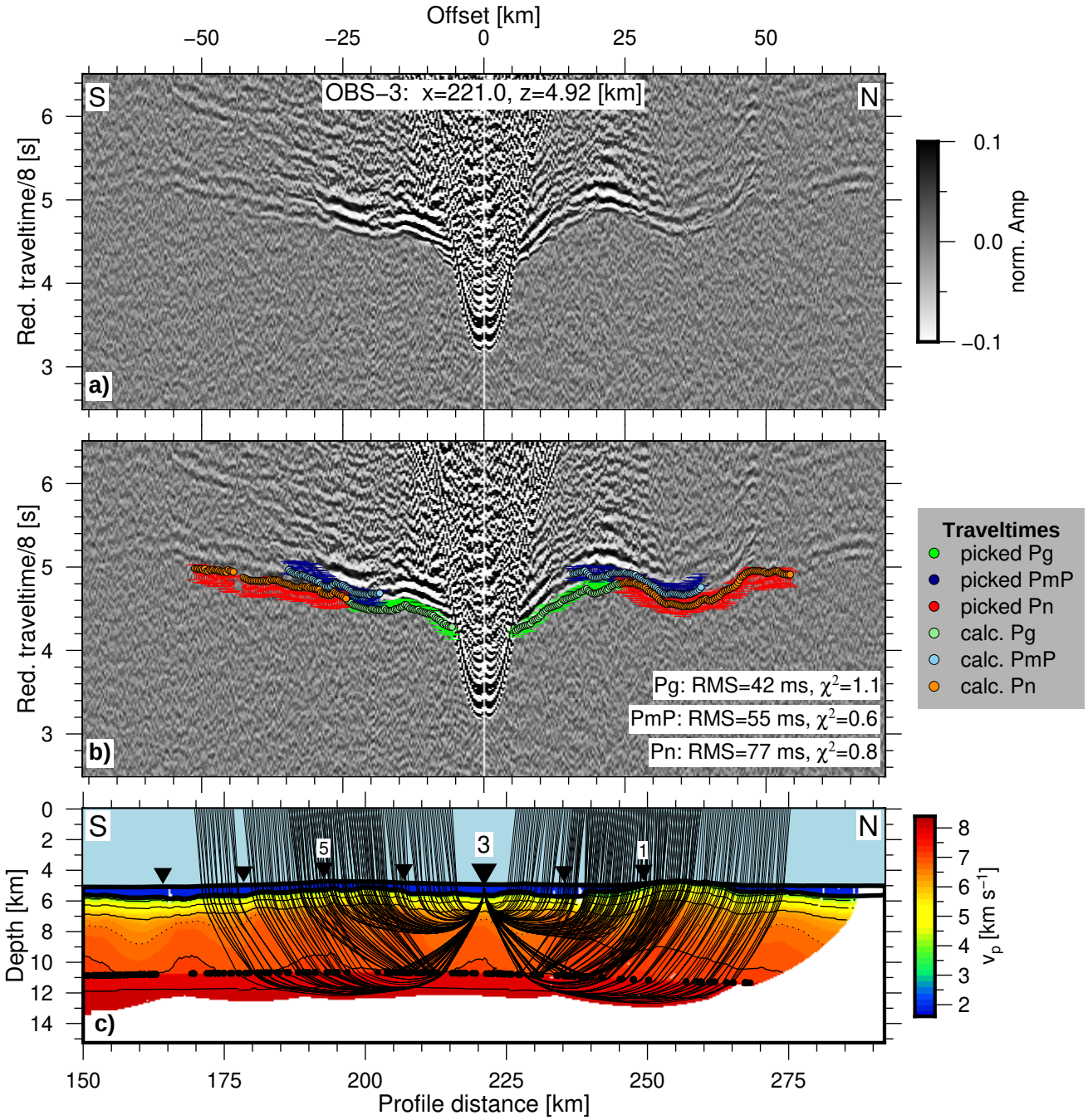

Figure S2c. Record section, traveltime fit and raypaths for OBS 03 (IS-01).

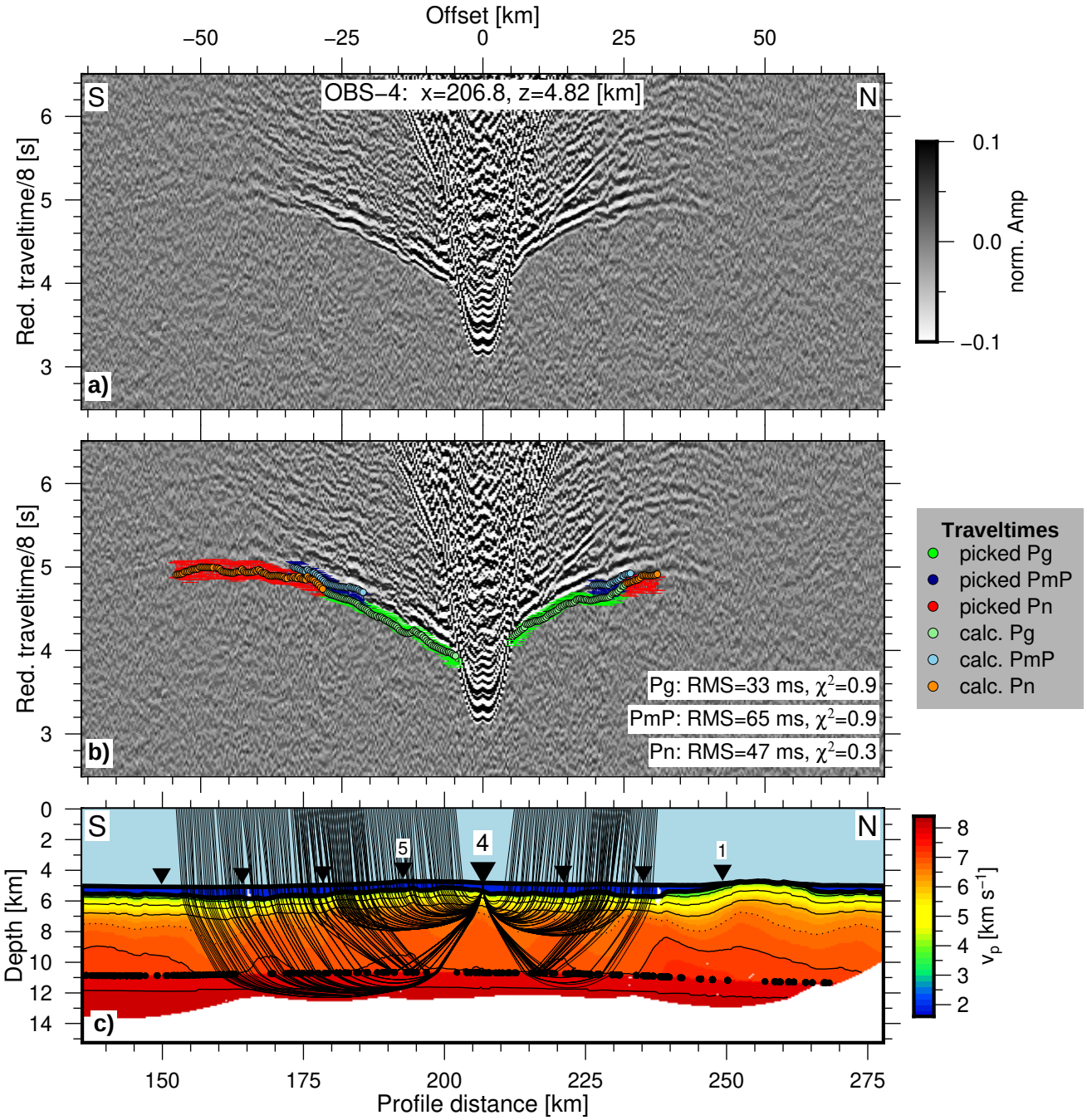

Figure S2d. Record section, traveltime fit and raypaths for OBS 04 (IS-01).

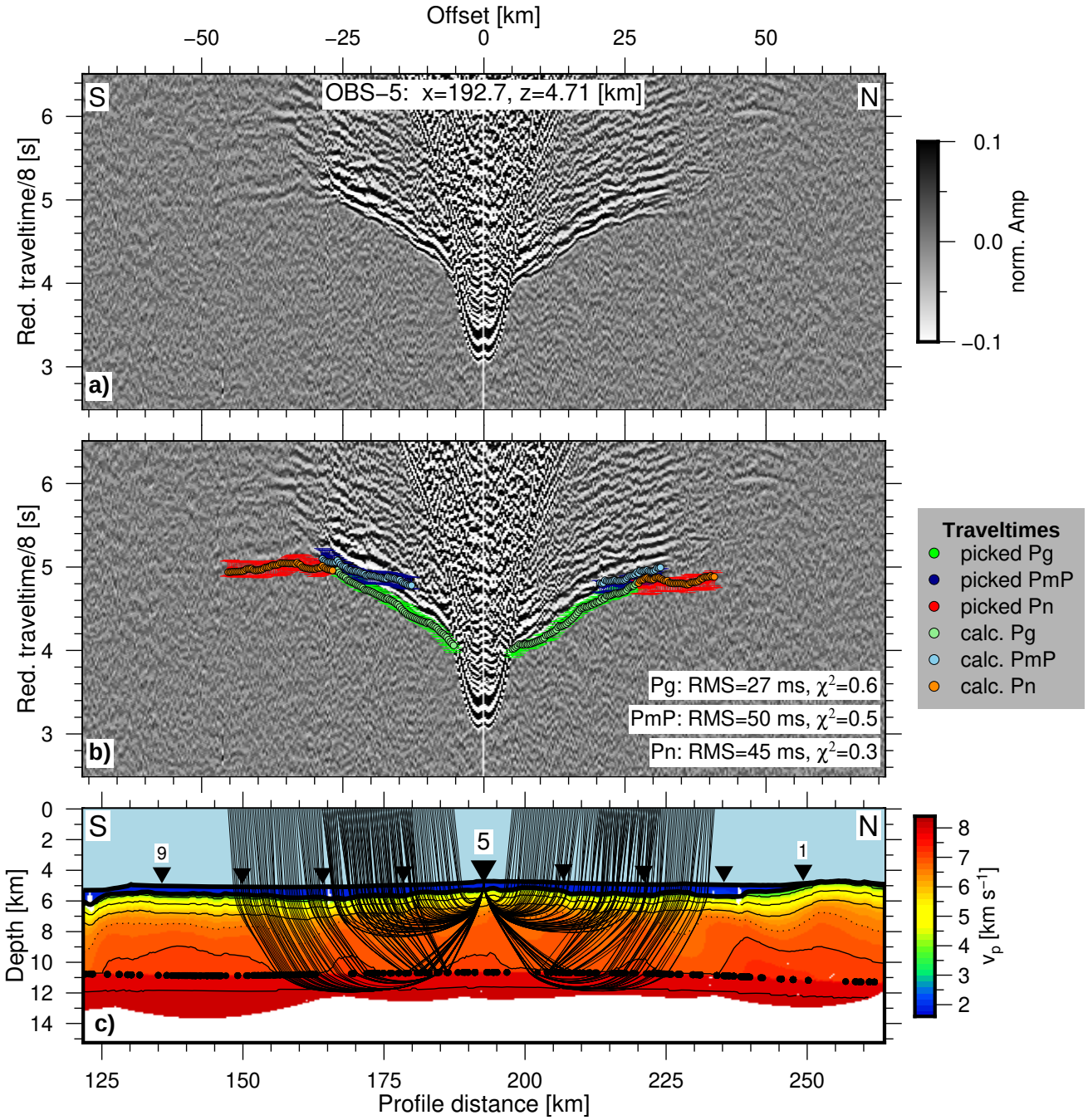

Figure S2e. Record section, traveltime fit and raypaths for OBS 05 (IS-01).

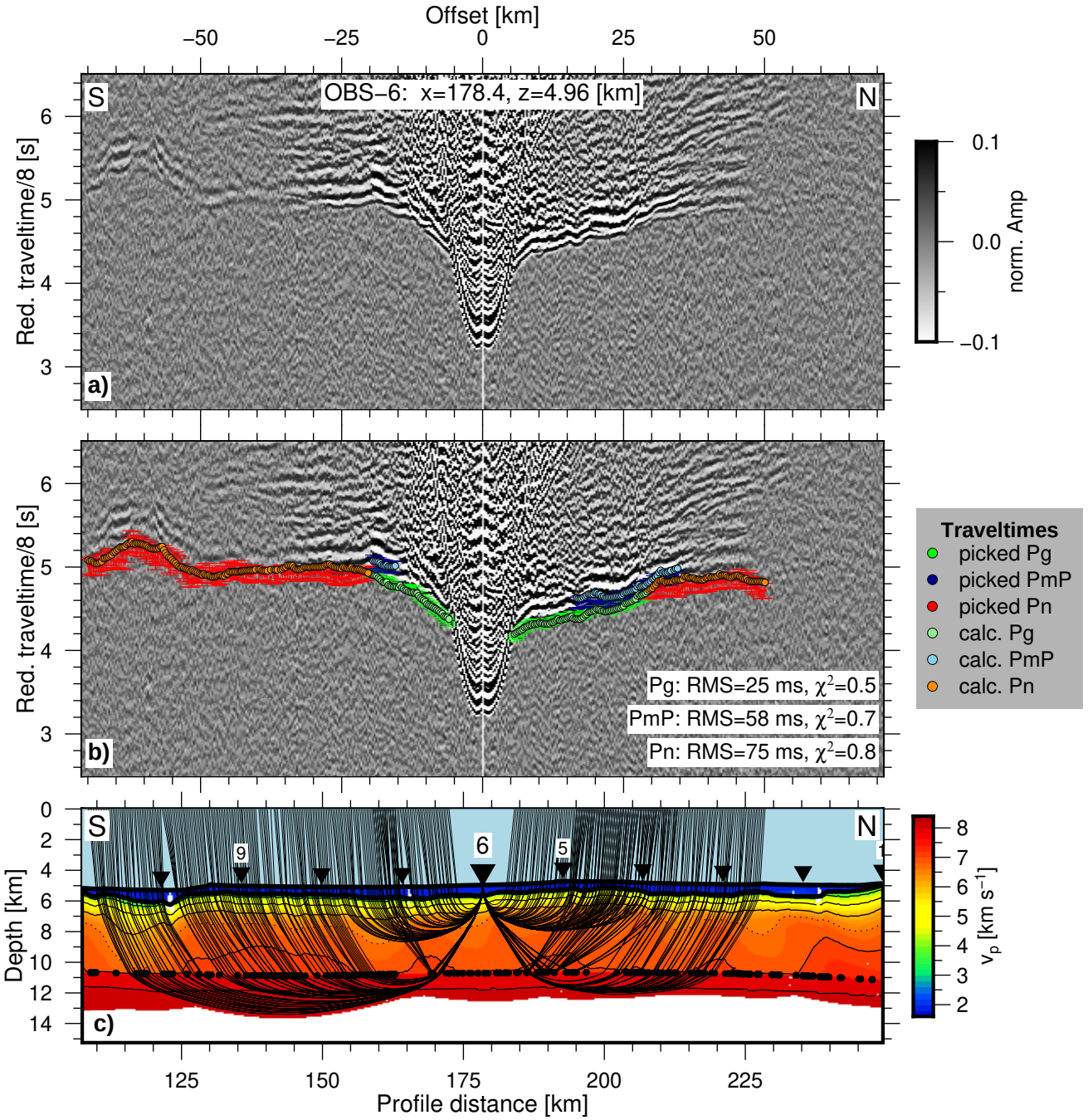

Figure S2f. Record section, traveltime fit and raypaths for OBS 06 (IS-01).

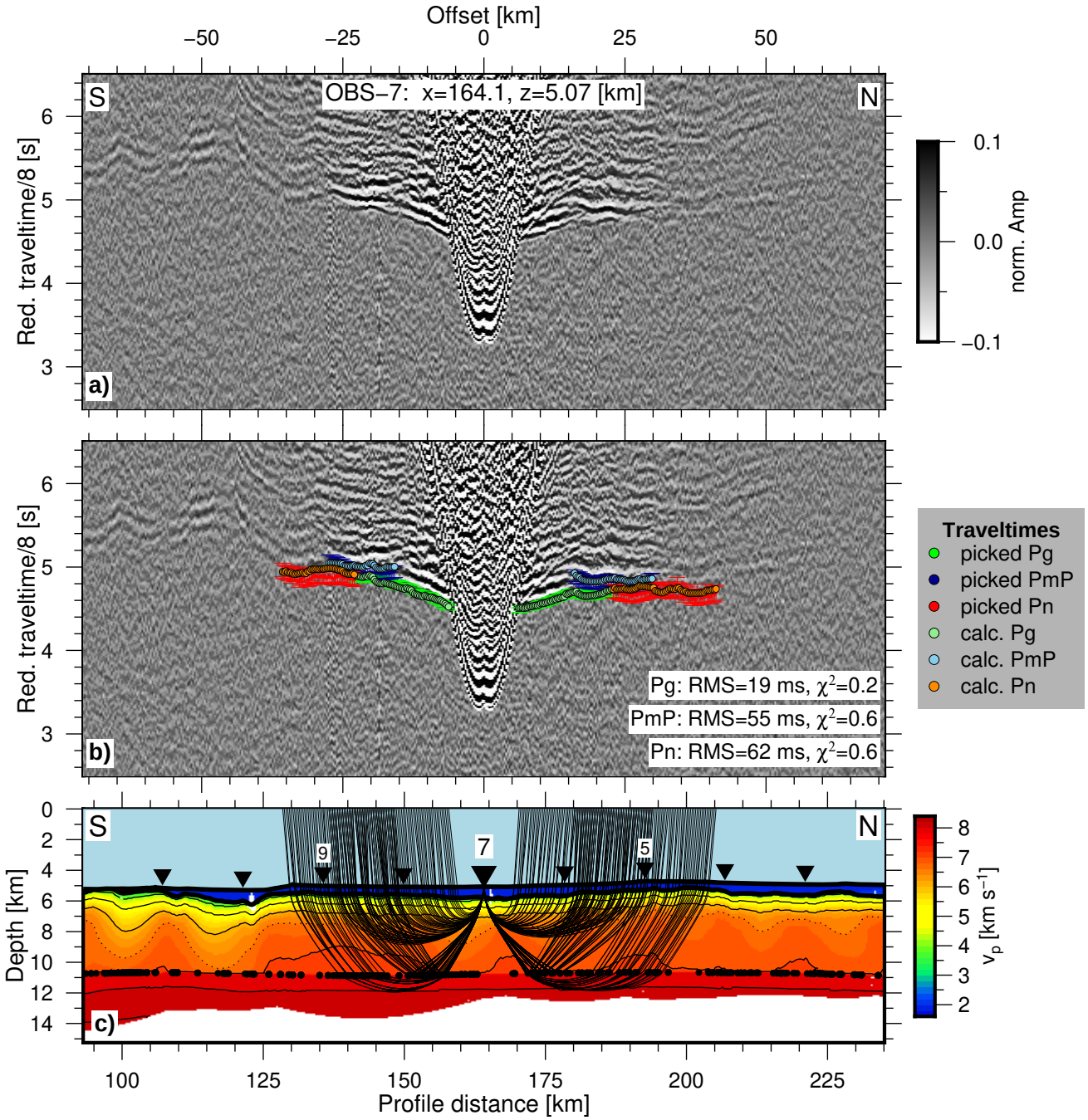

Figure S2g. Record section, traveltime fit and raypaths for OBS 07 (IS-01).

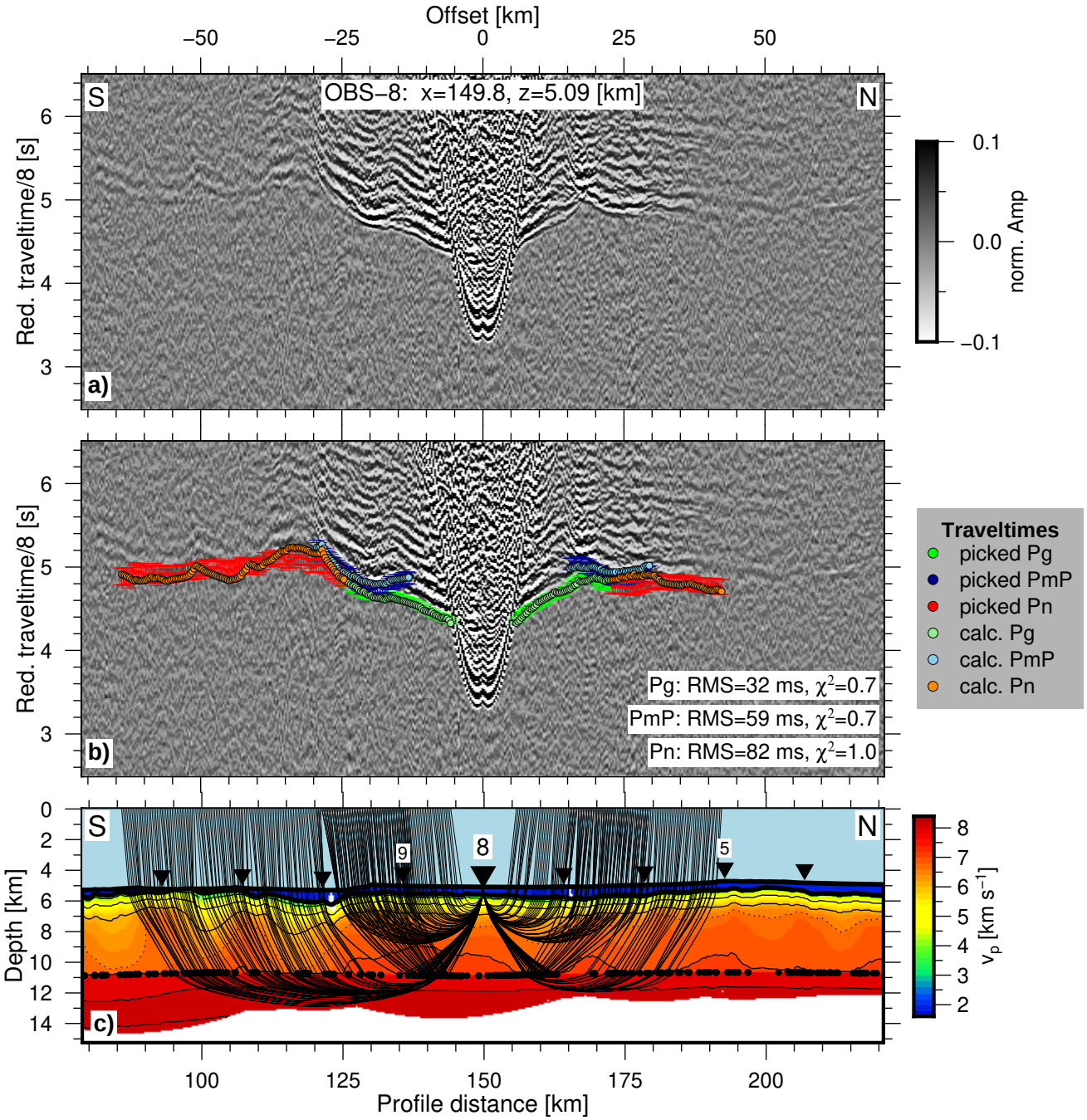

Figure S2h. Record section, traveltime fit and raypaths for OBS 08 (IS-01).

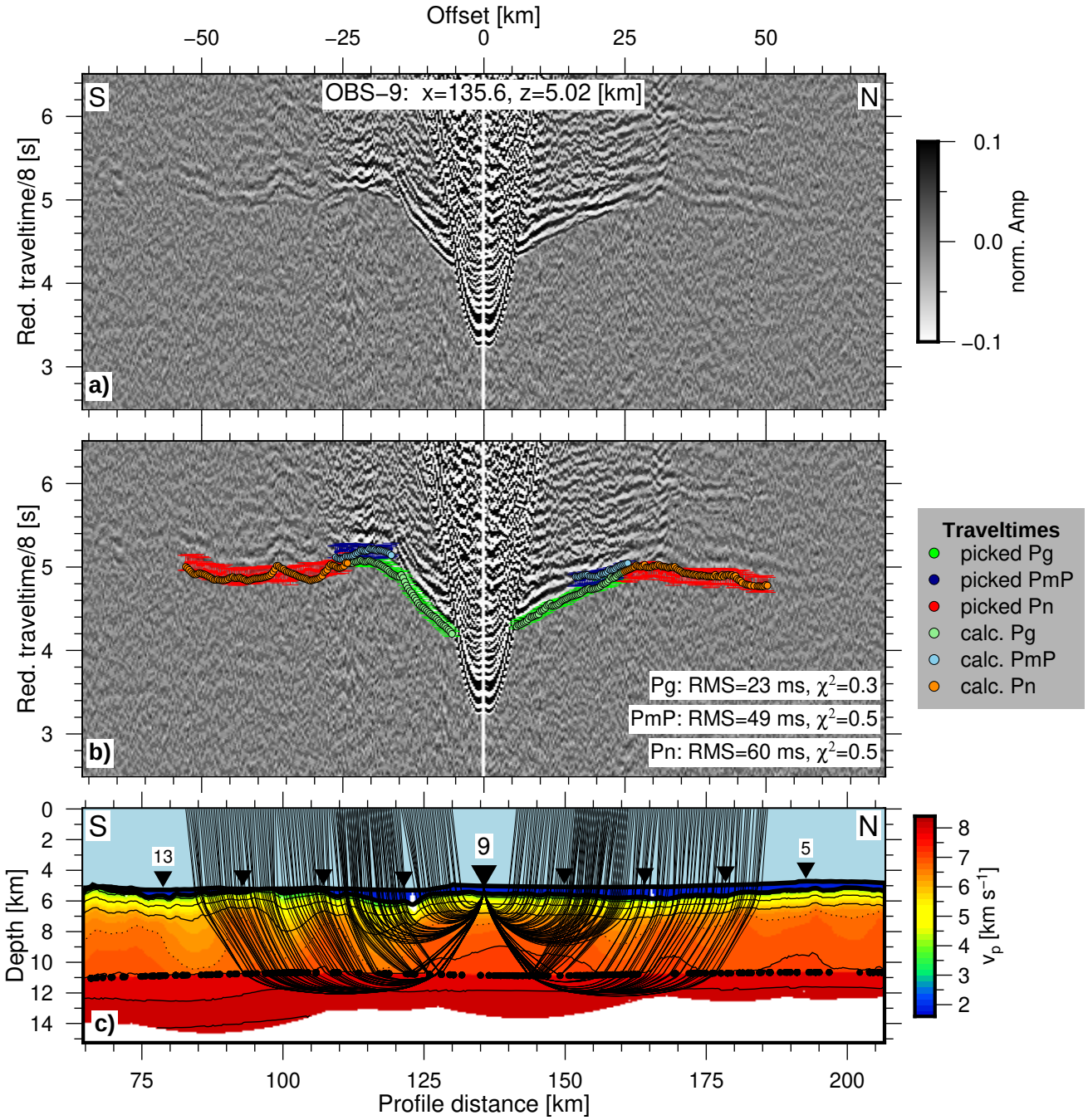

Figure S2i. Record section, traveltime fit and raypaths for OBS 09 (IS-01).

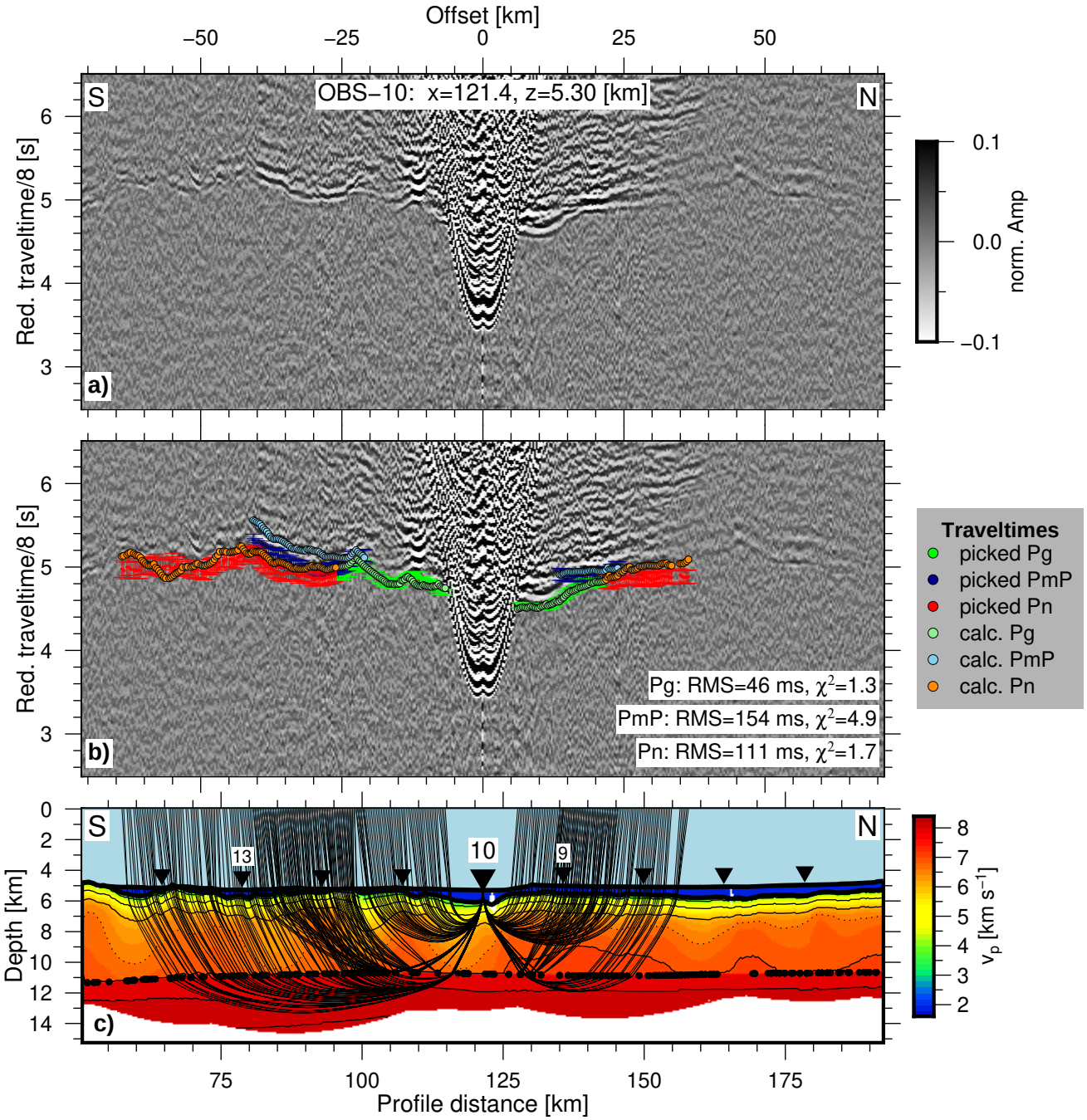

Figure S2j. Record section, traveltime fit and raypaths for OBS 10 (IS-01).

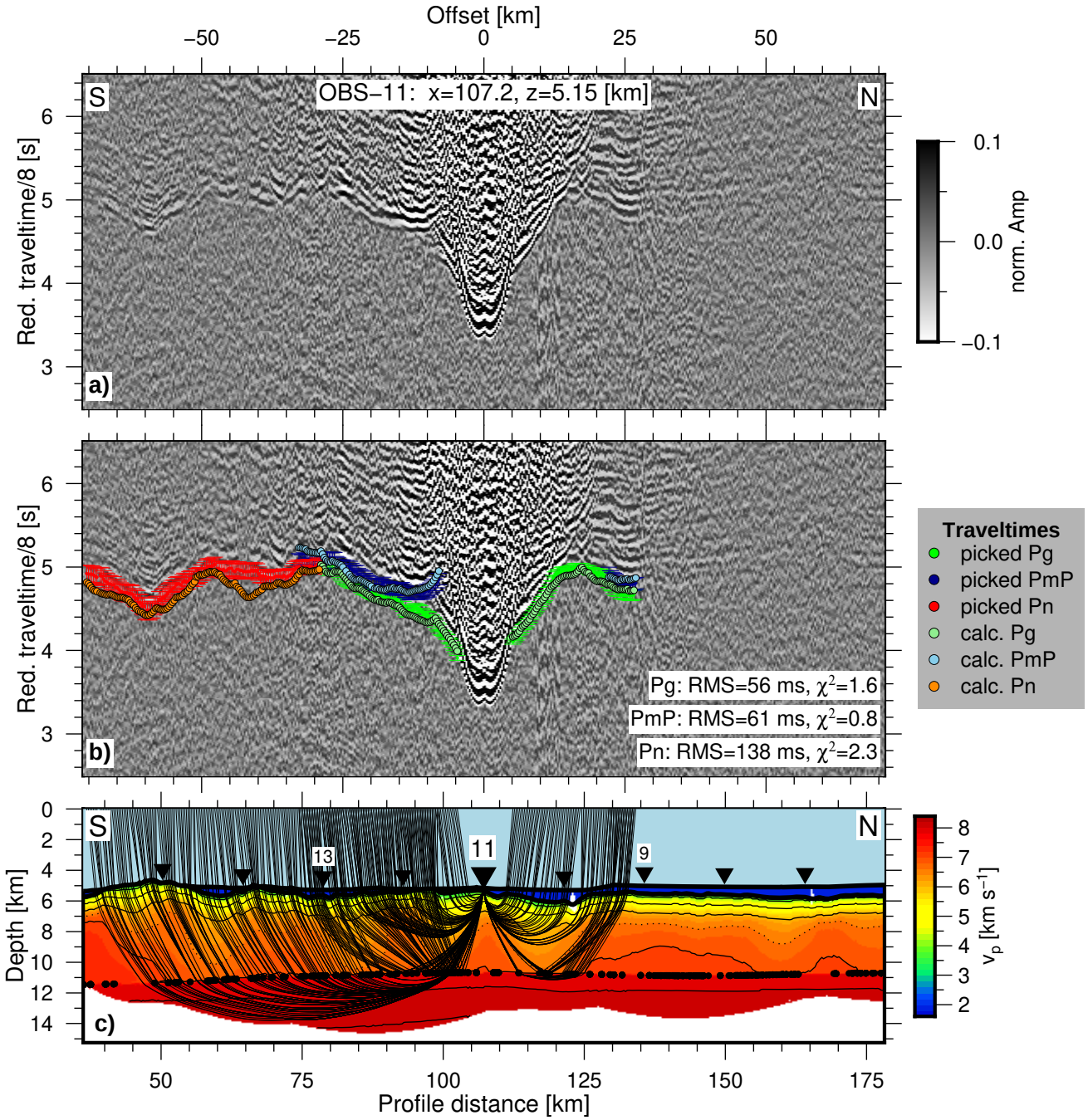

Figure S2k. Record section, traveltime fit and raypaths for OBS 11 (IS-01).

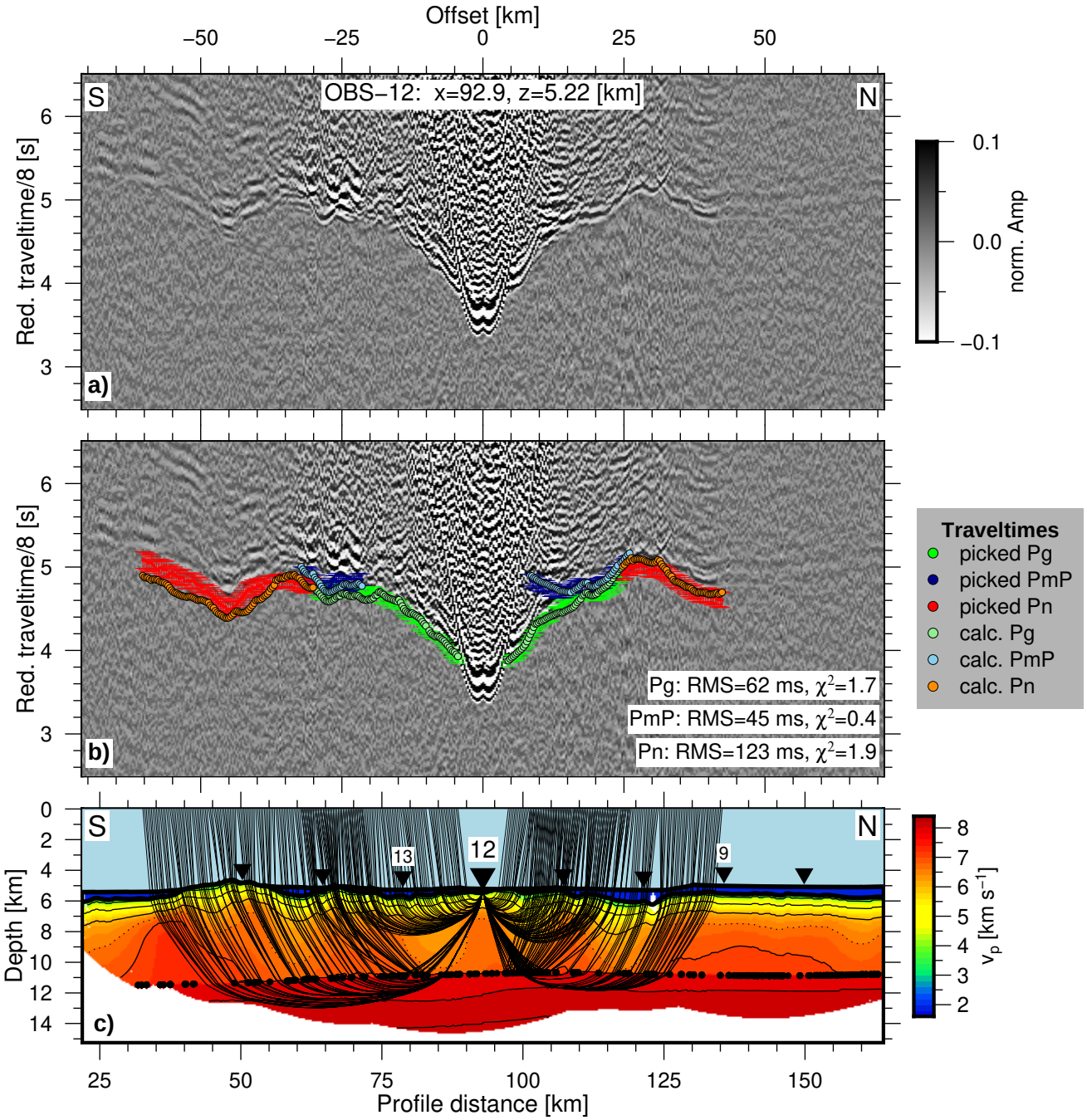

Figure S2l. Record section, traveltime fit and raypaths for OBS 12 (IS-01).

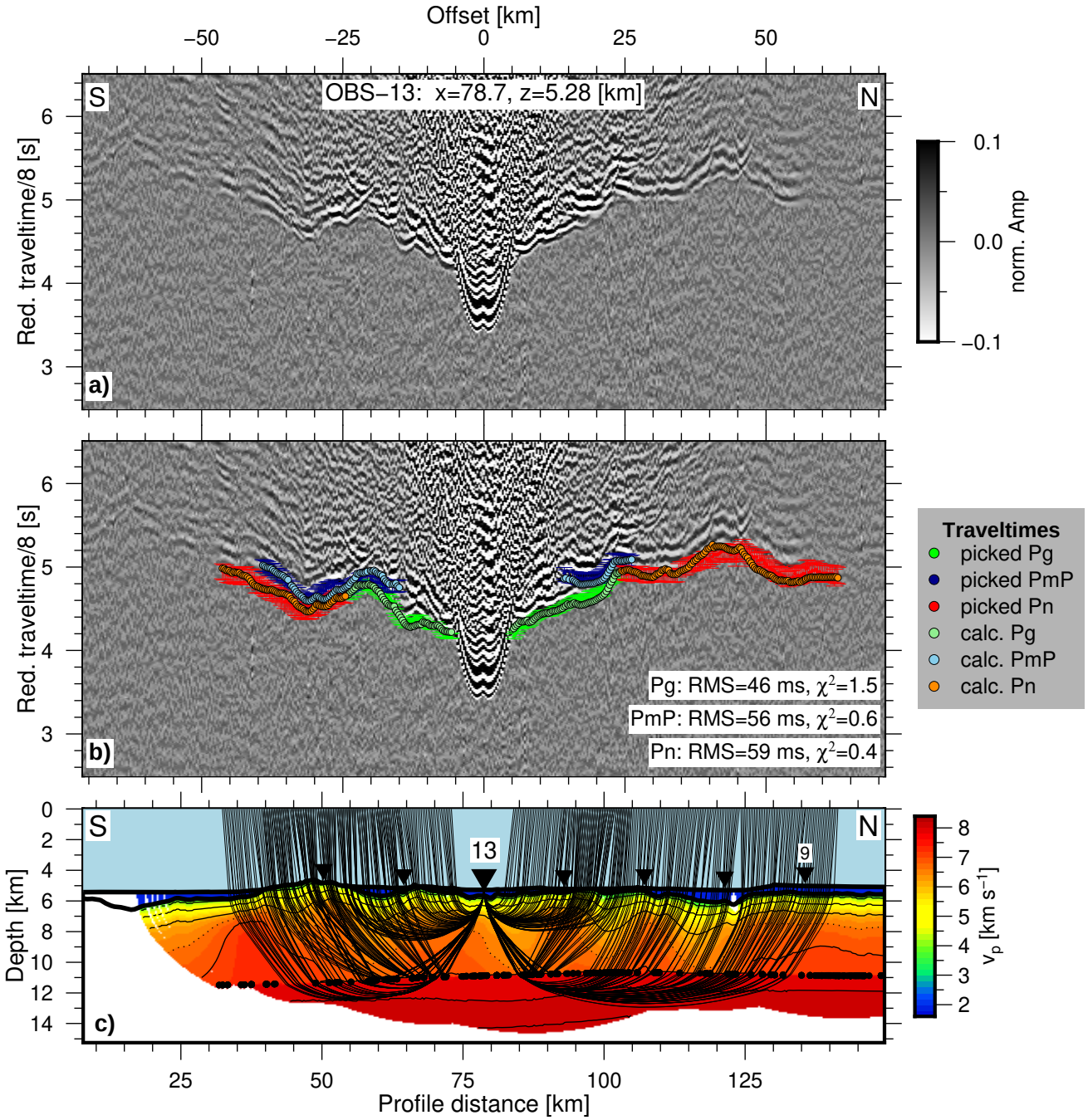

Figure S2m. Record section, traveltime fit and raypaths for OBS 13 (IS-01).

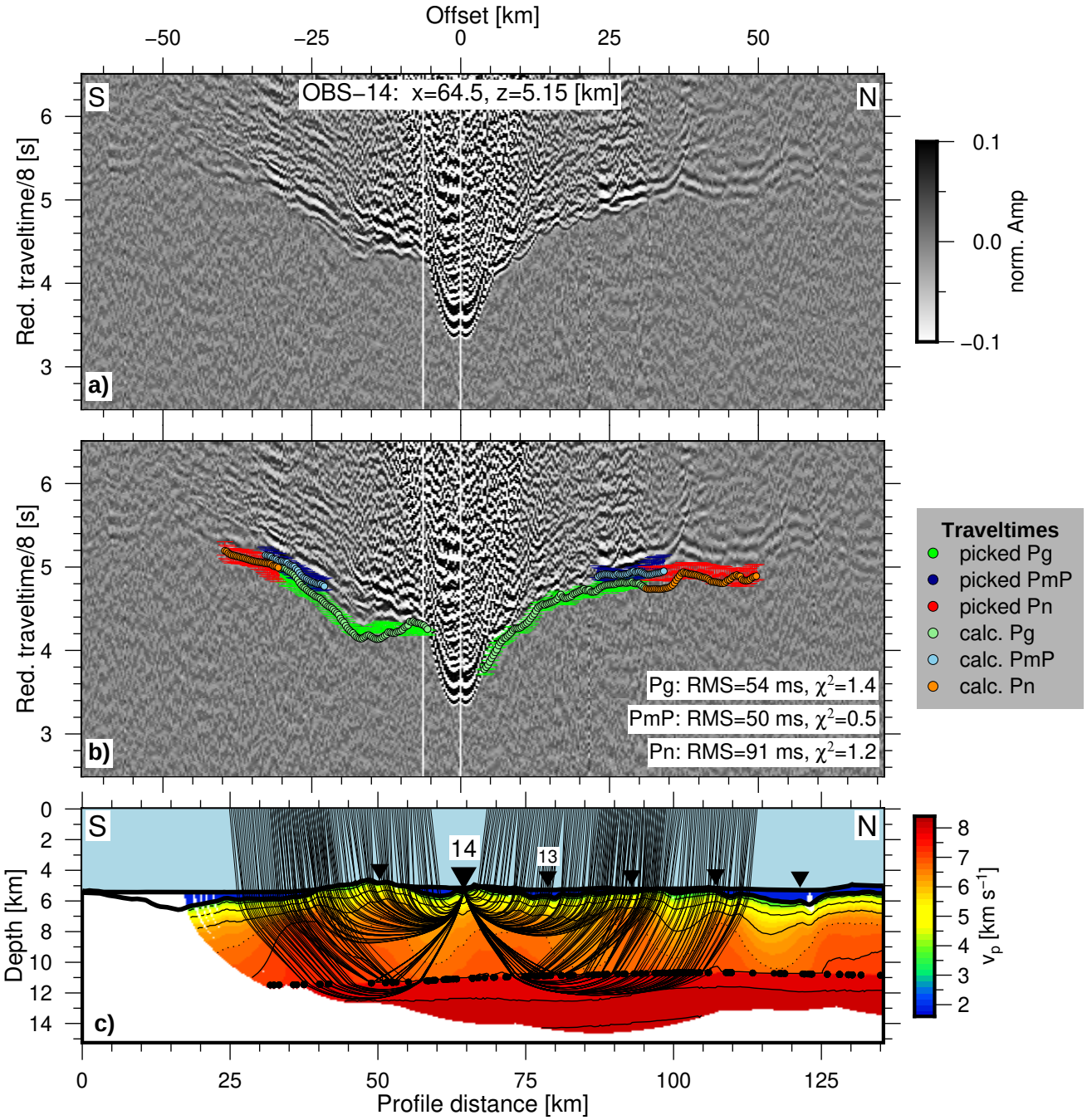

Figure S2n. Record section, traveltime fit and raypaths for OBS 14 (IS-01).

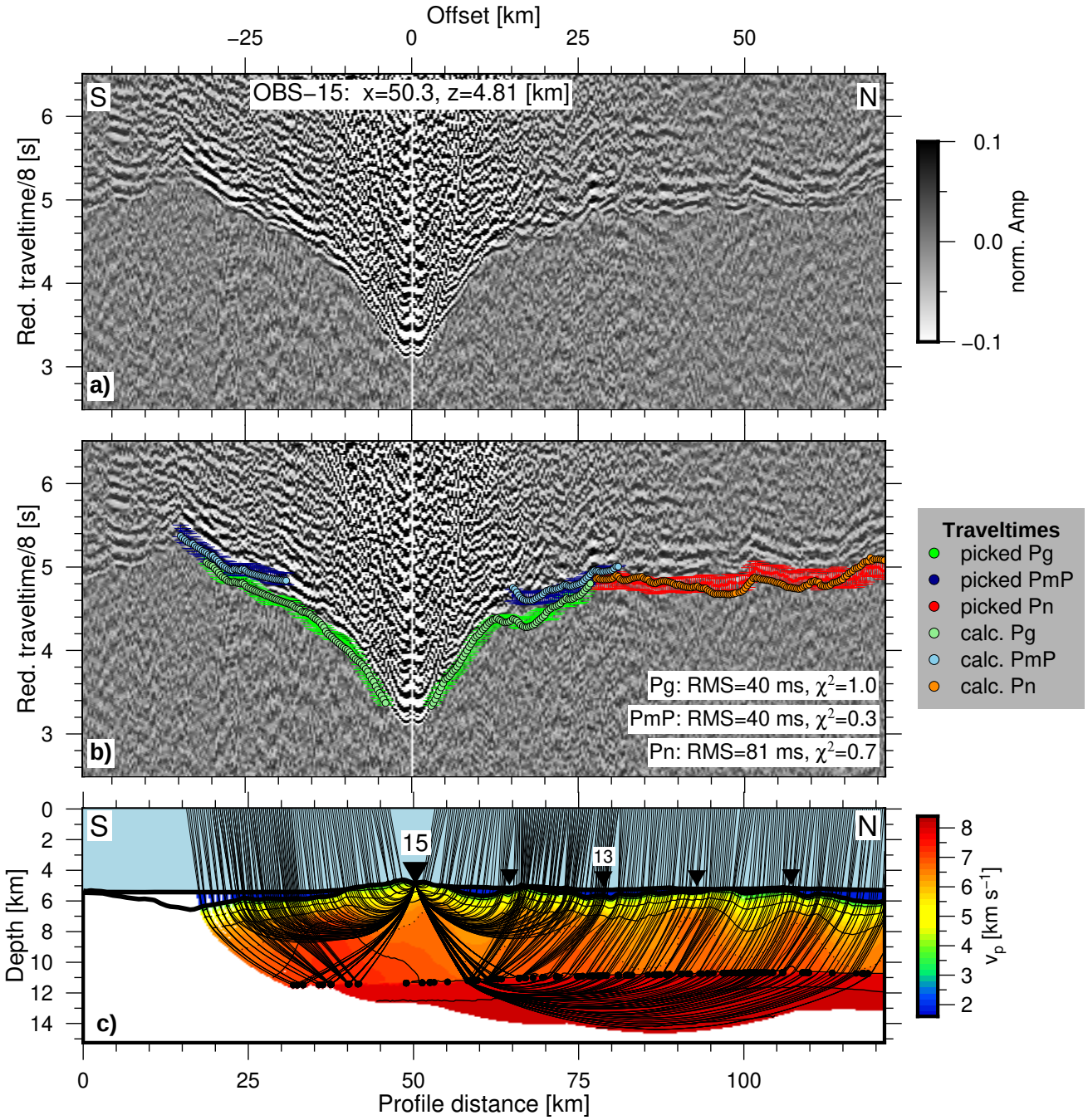

Figure S2o. Record section, traveltime fit and raypaths for OBS 15 (IS-01).

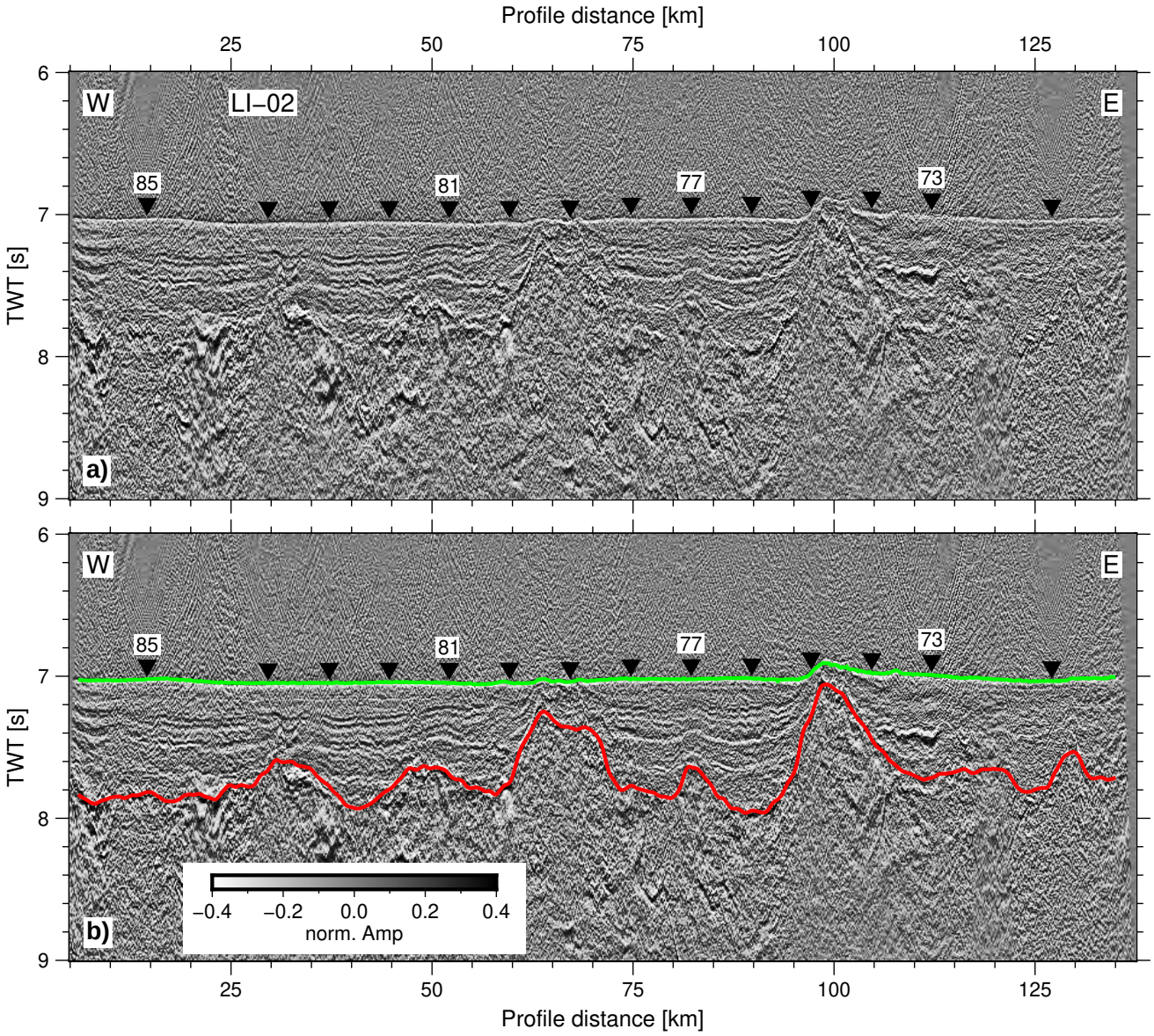

Figure S3. LI-02: **(a)** Mirror image obtained by migration of the multiples (e.g Grion et al., 2007) with **(b)** superimposed seafloor (green) and basement (red) picks. The amplitude is normalized by its maximum and clipped to 40 %.

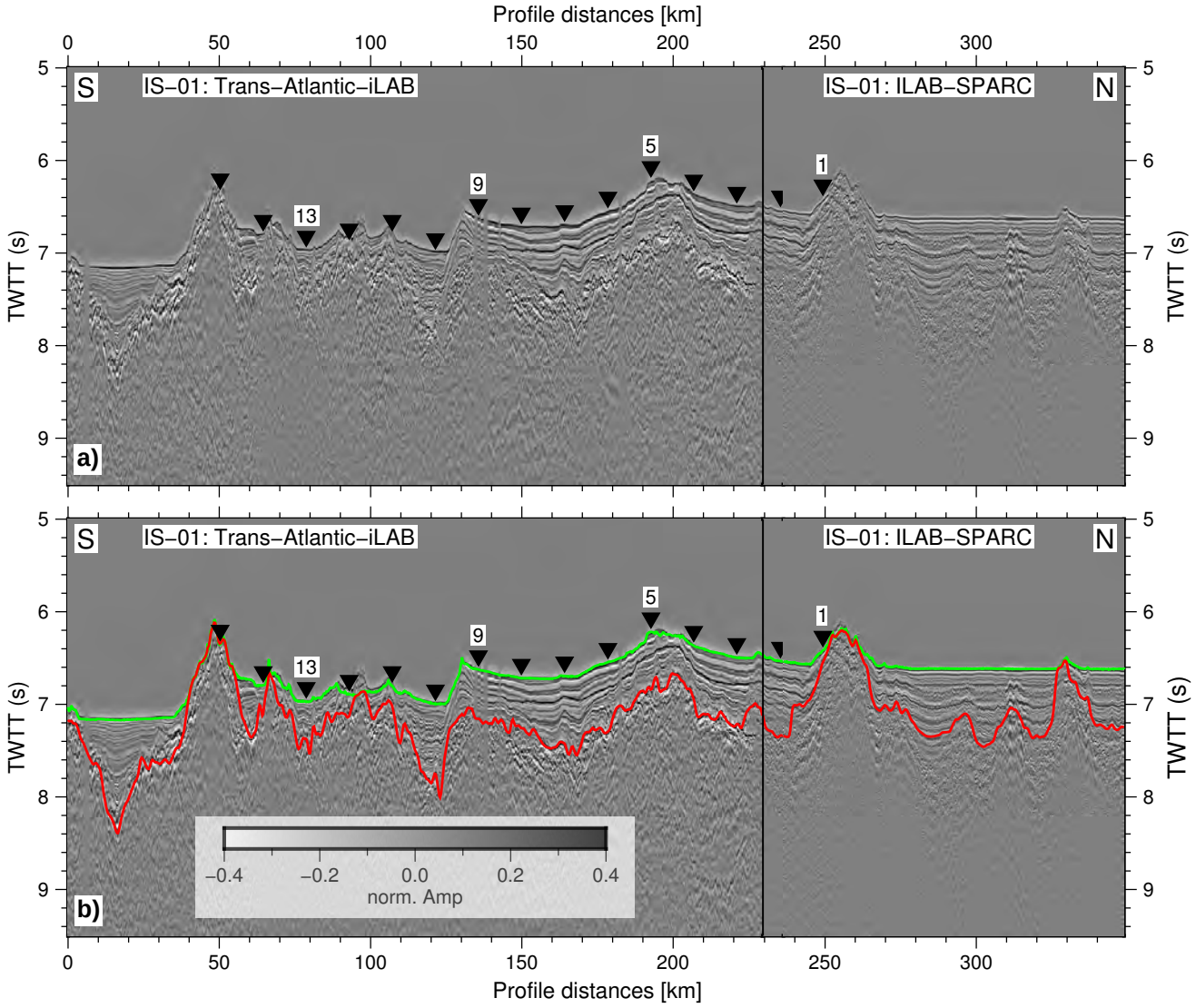

Figure S4. IS-01: **(a)** A composite post-stack time-migrated MCS section along the N-S line acquired during the two cruises, Trans-Atlantic-iLAB (2015) and ILAB-SPARC (2018). The solid vertical line indicates the joint location for the two datasets. The information on the MCS data processing steps is provided in the main text. The amplitude is normalized by its maximum and clipped to 40 %. **(b)** Seafloor (green) and basement (red) picks are superimposed on the seismic section.

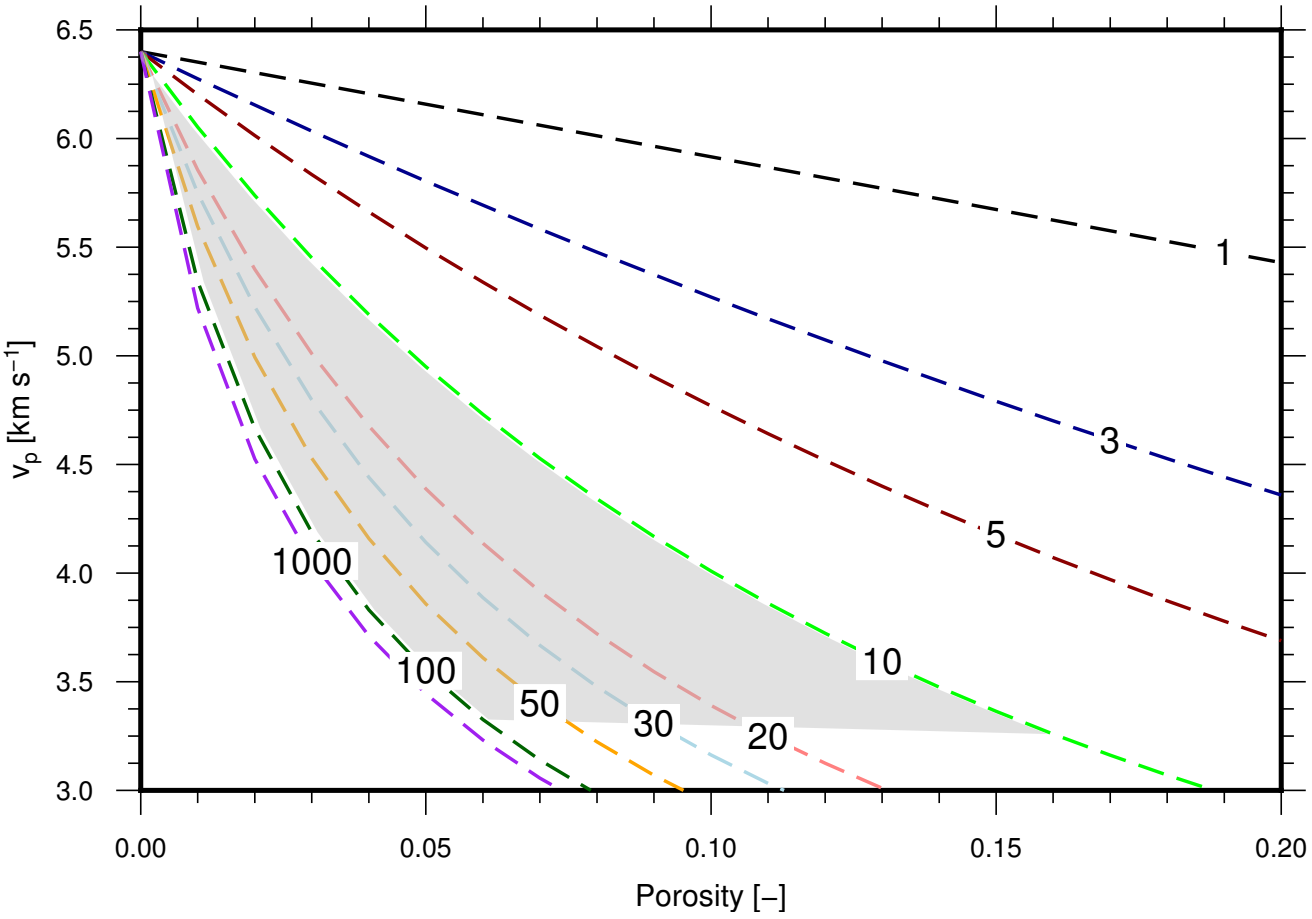

Figure S5. Velocity-porosity relationship for different aspect ratios of fractures (numbered labels). Calculated using a differential effective medium analysis after Taylor and Singh (2002) for a basaltic host rock. Grey area highlights the range of observed crustal velocities and hence the range of possible porosities with respect to the chosen range of aspect ratios of 10-100.

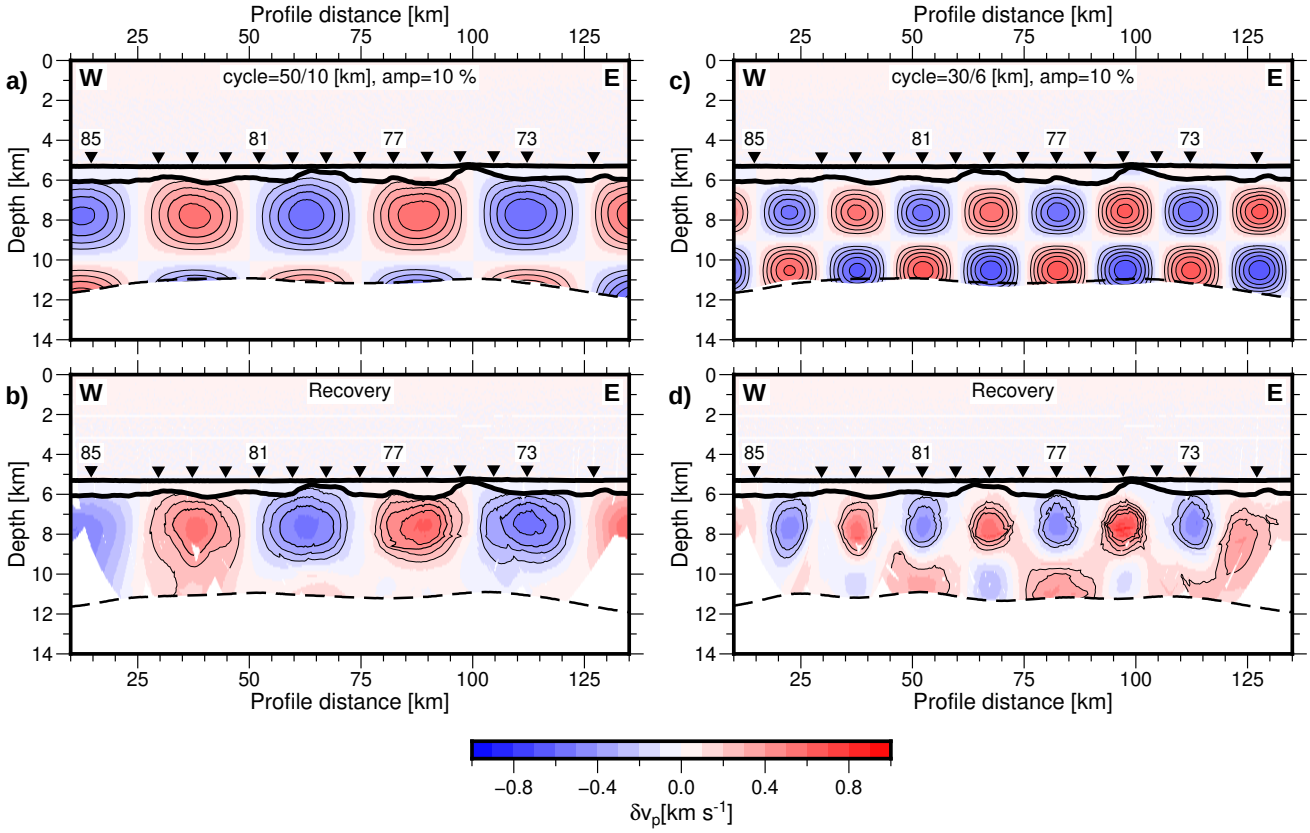

Figure S6. Checkerboard test for LI-02: crustal checkerboard resolution test for different cycle lengths and a perturbation amplitude of 10 %. The contour interval is 0.1 km/s starting at ±0.2 km/s. The dashed line denotes the constrained Moho reflector. The remaining figure elements are the same as in Figure 5 in the main text.

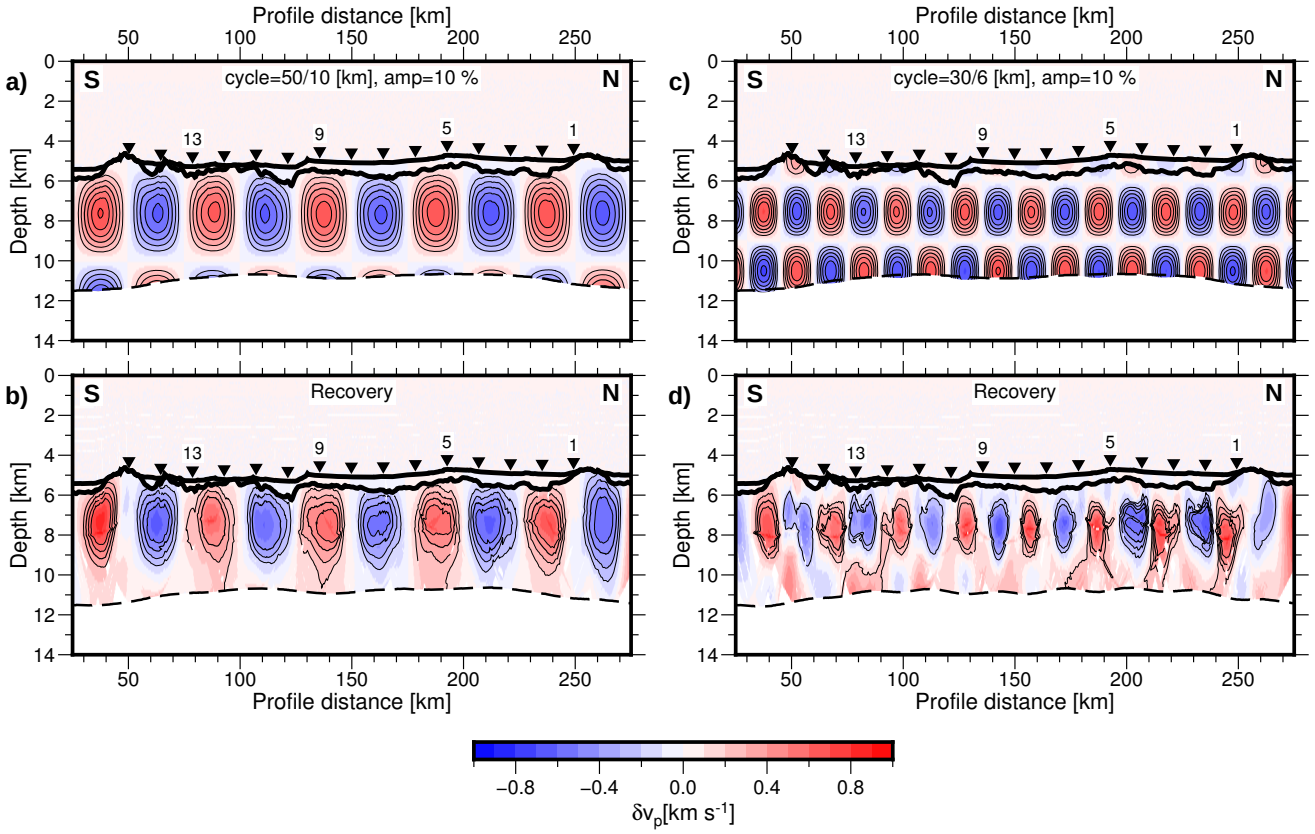

Figure S7. Checkerboard test for IS-01: checkerboard resolution test as in Fig. S6.

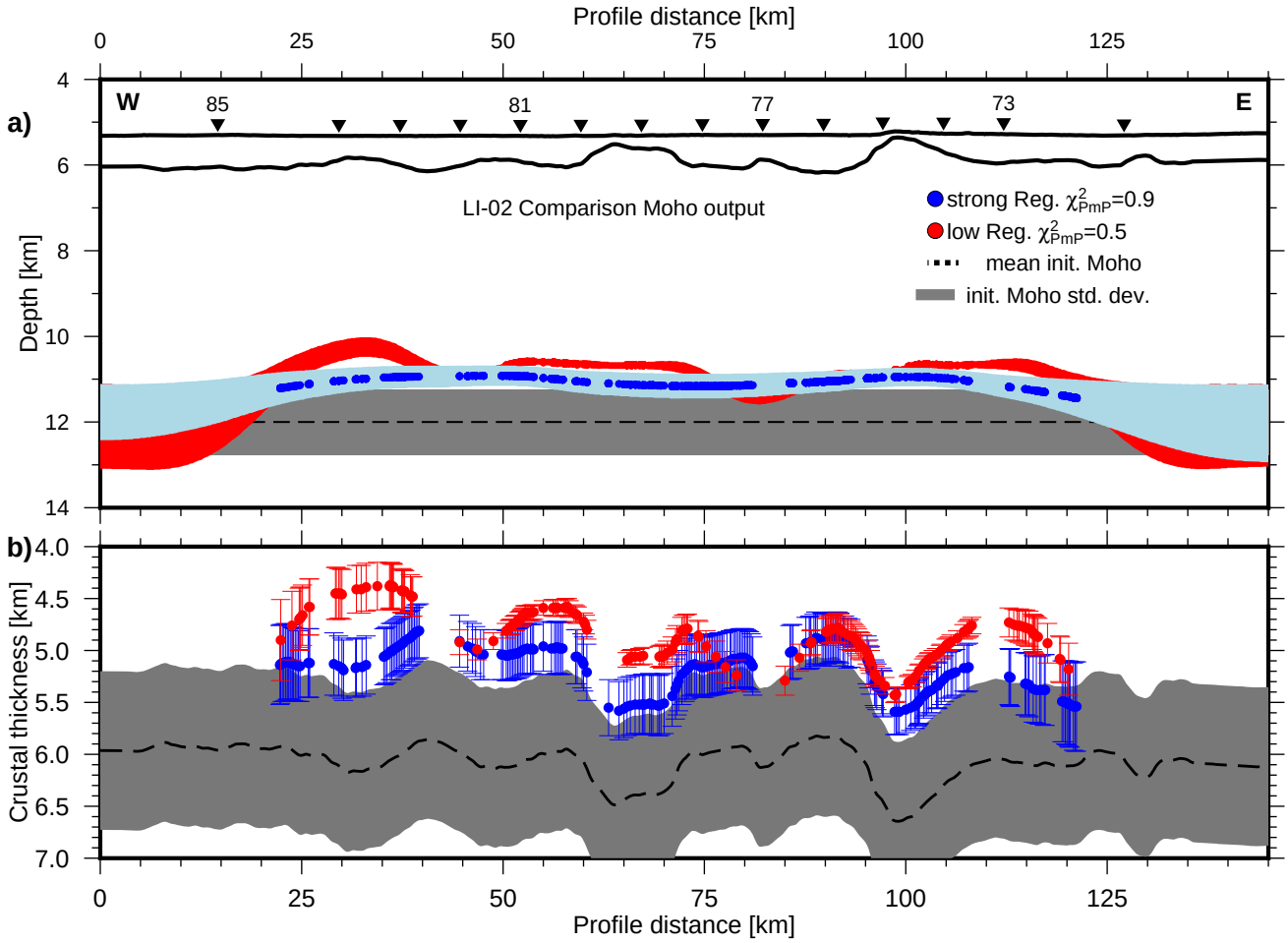

Figure S8. LI-02: **(a)** Comparison of Moho results for line LI-02 from the MCAs using 'strong' (blue) and weak regularization (see Table S3). Dots and shaded areas denote the mean obtained reflection points and the Moho standard deviation from the MCA. Dashed line and gray shading denote the mean initial Moho and the input standard deviation. Solid black lines denote the seafloor and the basement. The inverted black triangles denote the OBS locations. Every fourth OBS is labeled. **(b)** Corresponding crustal thickness along the line. The dots and the error bars represent the modelled PmP reflection points and their standard deviation.

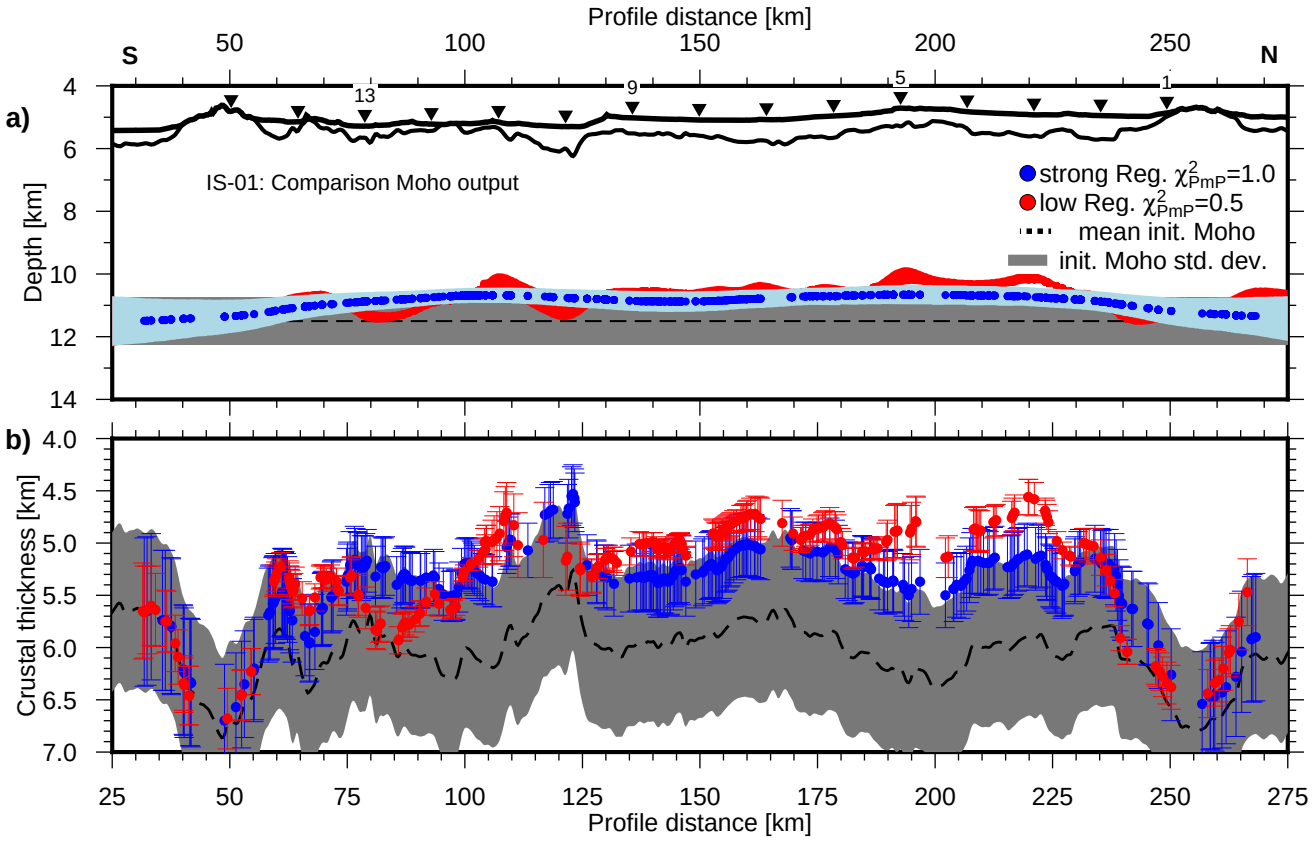

Figure S9. IS-01: the same comparison as in Fig. S8 but for line IS-01.

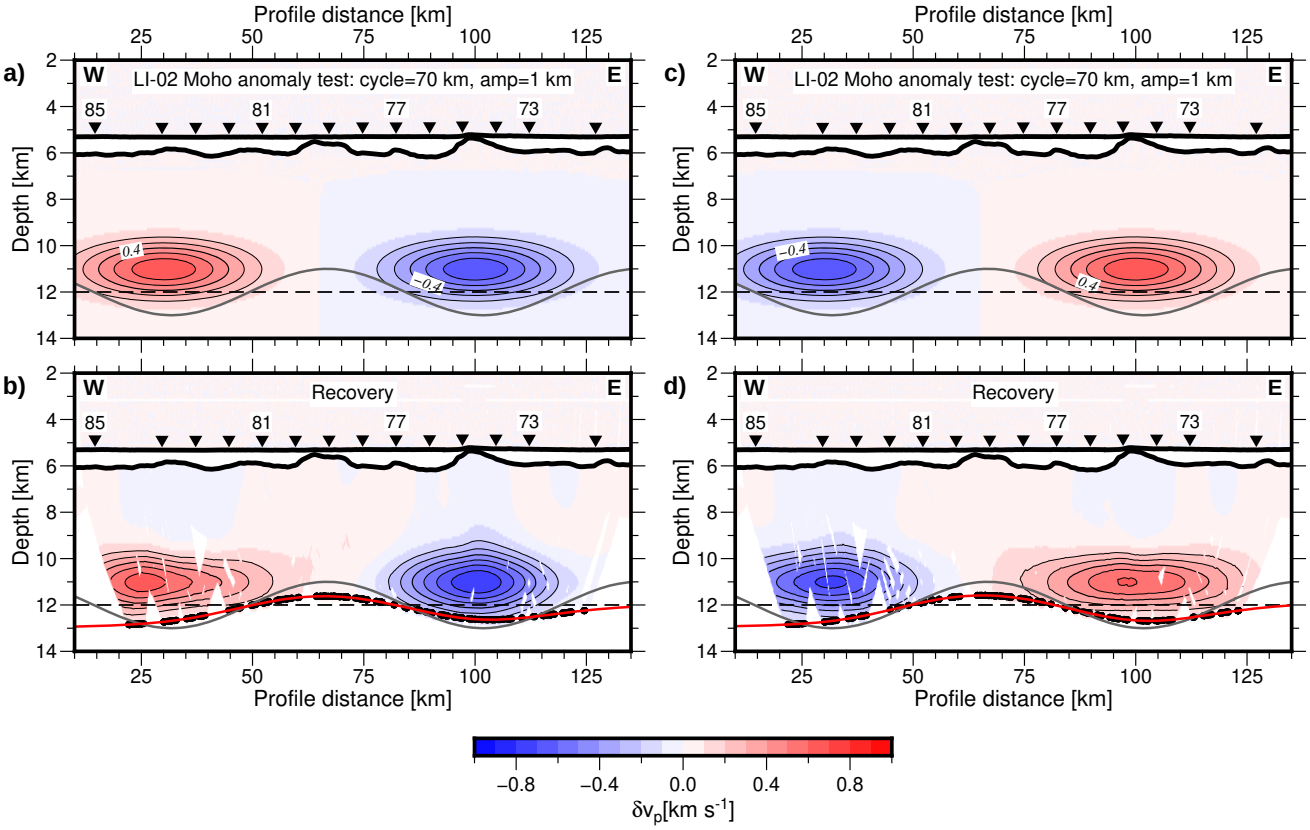

Figure S10. LI-02: Resolution test for sinusoidal Moho anomaly with a cycle of 70 km and a perturbation amplitude of 1 km. Additionally, we introduced gaussian velocity anomalies with horizontal radius of 20 km, a vertical radius of 1.25 km and a perturbation amplitude of 10 % above the Moho reflector. Panels (c,d) show the same test with reversed polarity of (a,b). The contour interval is 0.1 km/s starting at 0.2 km/s. The horizontal dashed, the grey and red lines and the black dots denote the mean input reflector, the perturbed input reflector and the recovered reflector with its obtained reflection points, respectively.

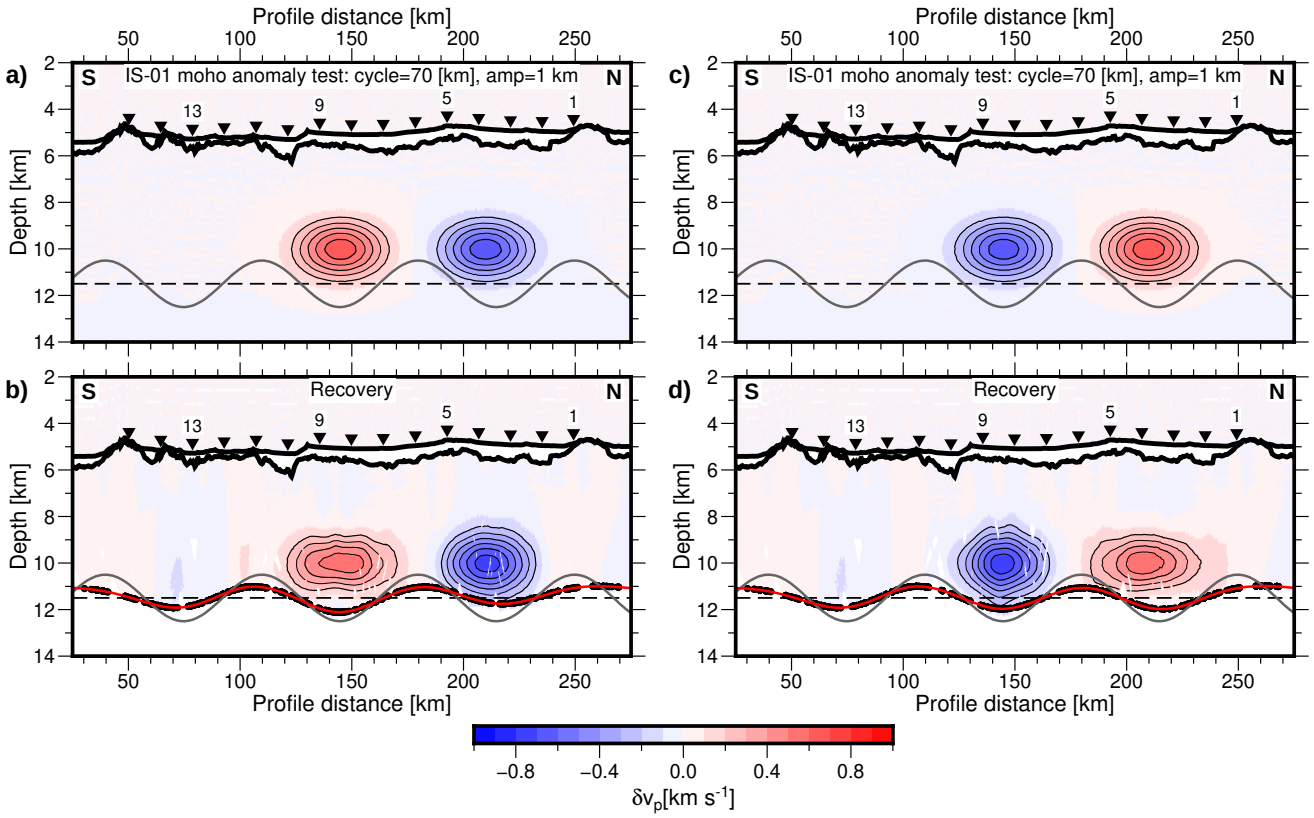

Figure S11. Moho resolution test for IS-01: the same test procedure and figure elements as in Figure S10.

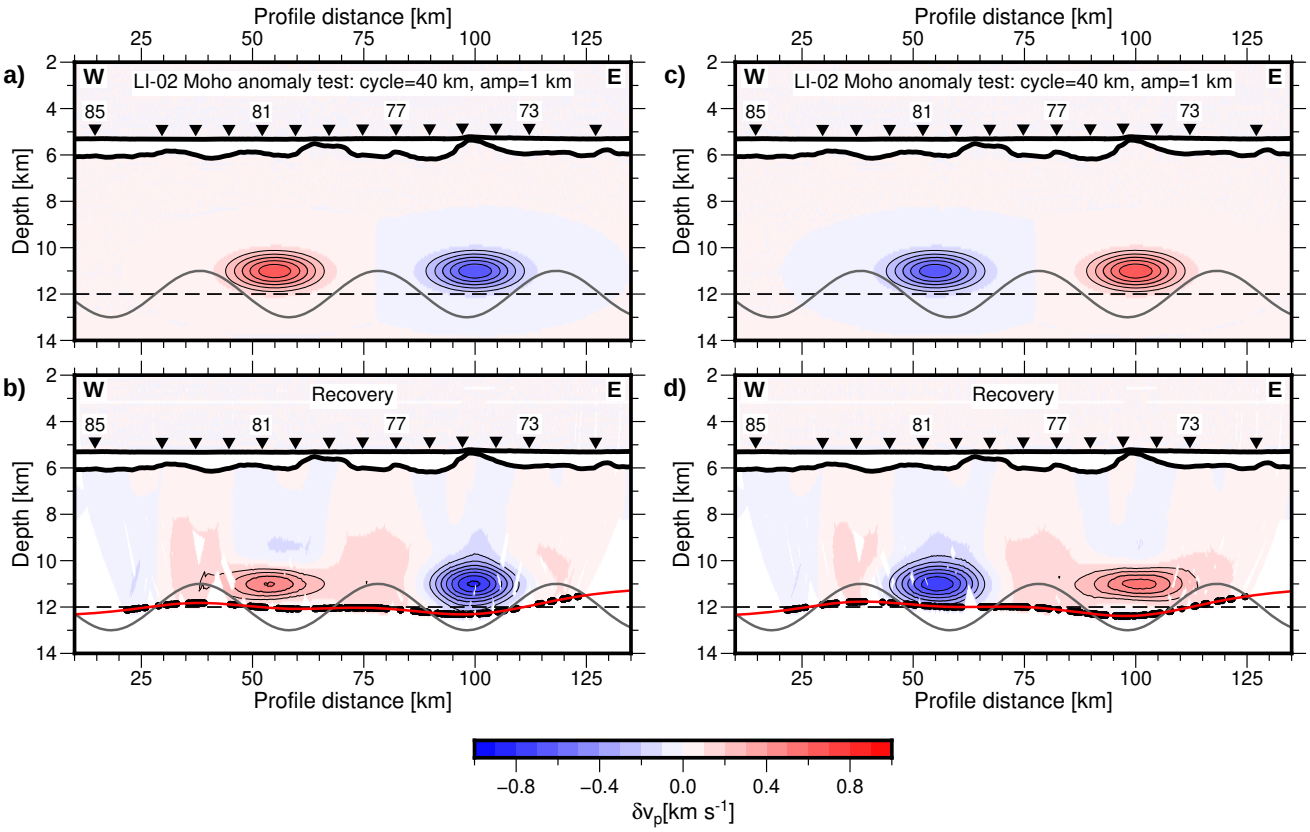

Figure S12. Moho resolution test for LI-02: the same test as in Fig. S10 but with a reduced reflector perturbation cycle length of 40 km.

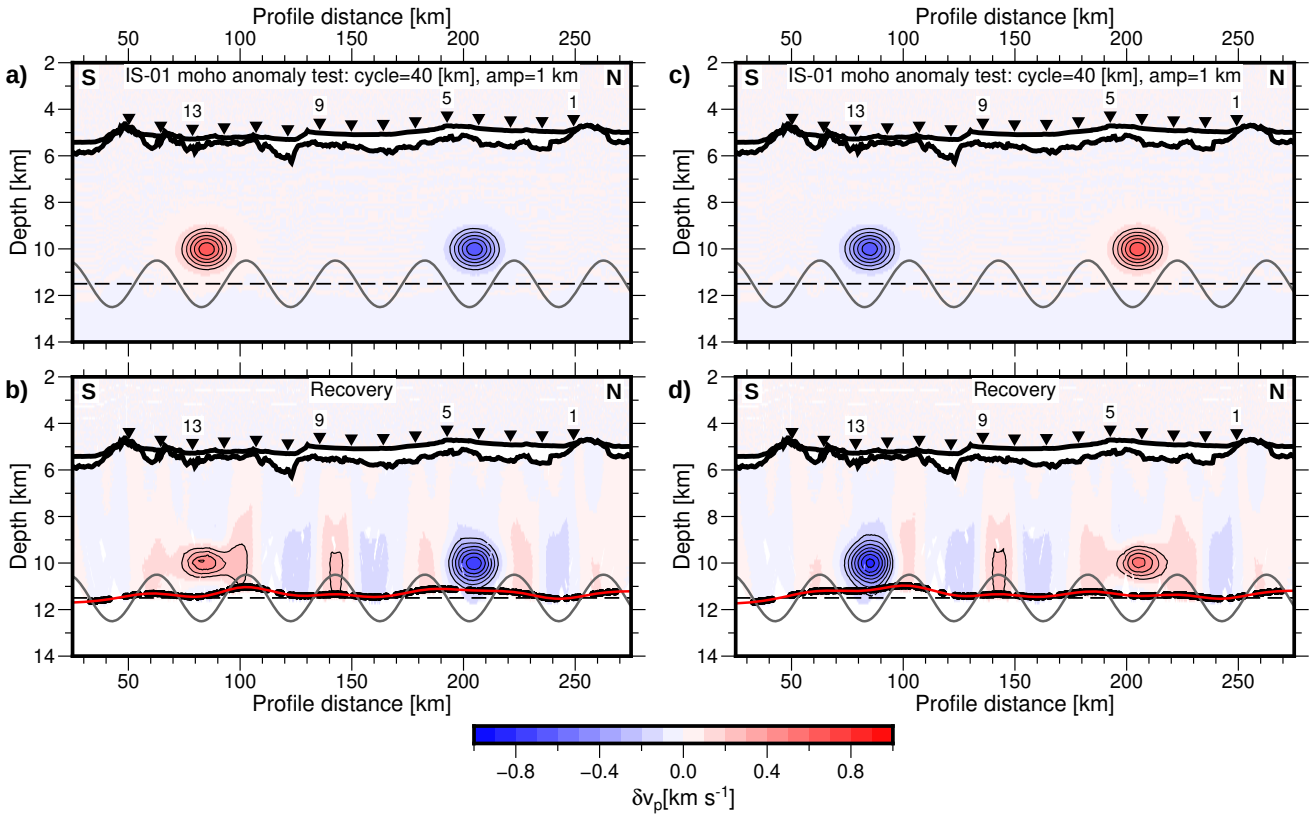

Figure S13. Moho resolution test for IS-01: the same test as in Fig. S11 but with a reduced reflector perturbation cycle length of 40 km.

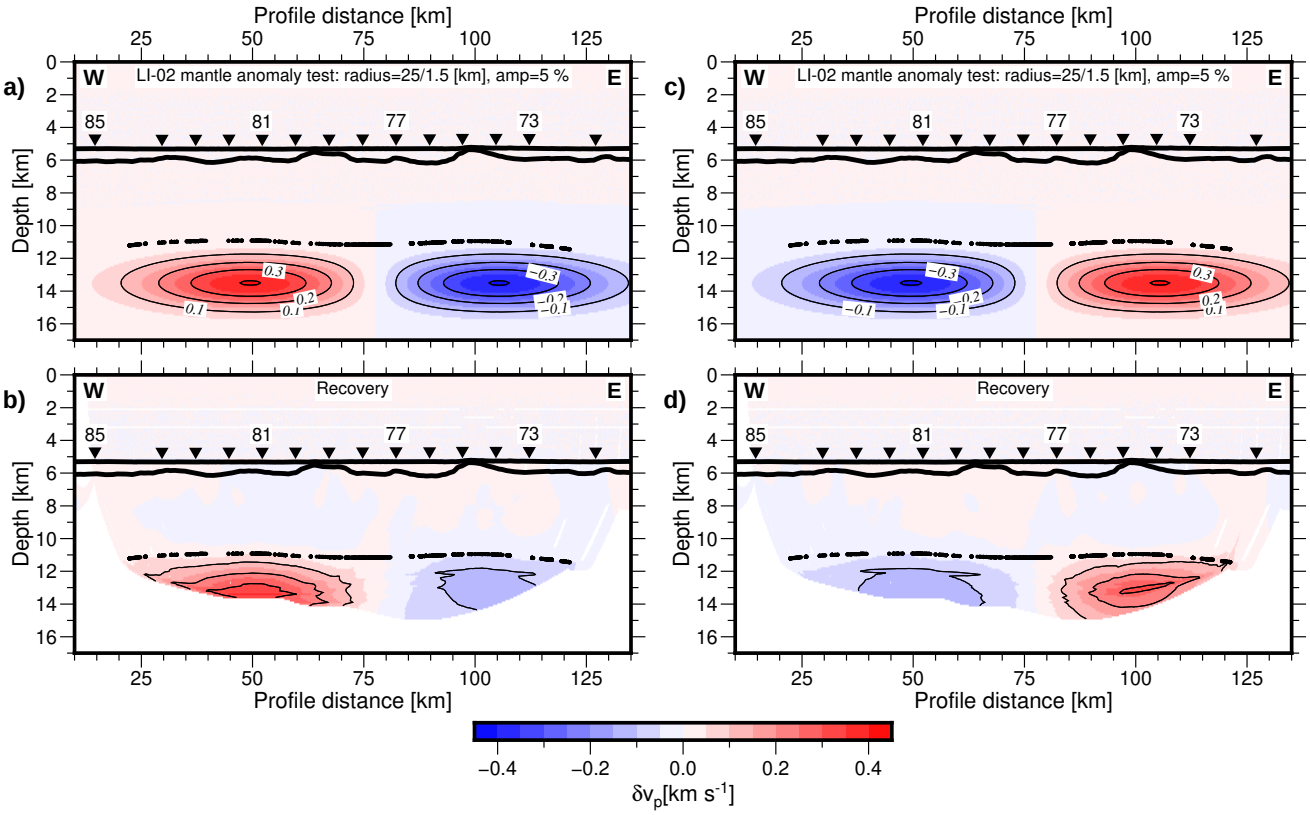

Figure S14. LI-02: mantle anomaly test for gaussian anomaly pattern with horizontal radius of 25 km, a vertical radius of 1.5 km and a perturbation amplitude of 5 %. Panels (c,d) show the same test with reversed polarity of (a,b) The contour interval is 0.1 km/s.

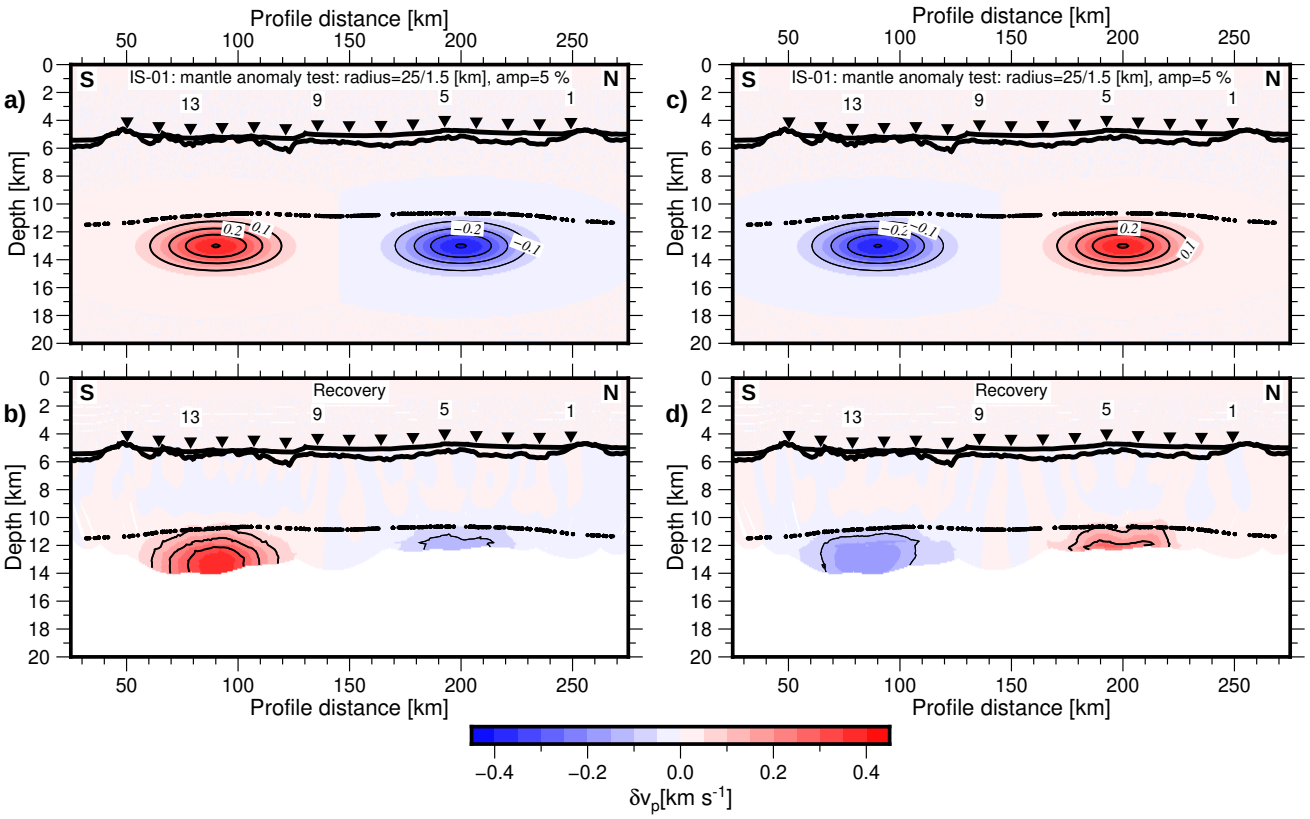

Figure S15. Mantle anomaly test for IS-01: the same testing procedure and figure elements as in Figure S14.

Table S2. Discretization, forward and inversion parameters used for the tomographic inversion with TOMO2D.

Parameter / Line	**LI-02**	**IS-01**
Discretizing		
profile length [km]	145	350
model depth [km]	20	20
horizontal velocity node spacing [km]	0.2	0.3
vertical velocity node spacing [km]	0.05 – 0.25, increasing with depth	
number of velocity nodes	102366	164547
horizontal reflector node spacing [km]	0.2	0.3
number of reflector nodes	726	1167
Forward modelling		
forward star	10x15	
max ray segment length [km]	1	
number of interpolation points per segment	8	
tolerance for conjugate gradient	4.00E-04	
tolerance for Brent minimization	5.00E-05	
Inversion		
horizontal correlation length for velocity [km]	1.25 – 5	1.5 – 5
vertical correlation length for velocity [km]	0.375 – 3	0.5 – 3
horizontal correlation length for reflector [km]	3	
velocity smoothing weight for Pg	30	30
velocity damping weight for Pg	30	30
velocity smoothing weight for Pg+PmP	50	70
velocity damping weight for Pg+PmP	50	50
reflector depth smoothing weight	50	70
reflector depth damping weight	50	50
depth kernel weighting factor	1	
velocity smoothing weight for Pg+PmP+Pn	100	100
velocity damping weight for Pg+PmP+Pn	500	300
max iteration Pg1	8	
max iteration Pg2	8	
max iteration Pg3	8	
max iteration PmP	8	
max iteration Pn	5	
target $\chi 2$	1.2	
tolerance for LSQR sparse matrix solver	3.00E-03	
number of initial models for MCA	100	
mean initial crustal thickness [km]	6	
velocity input standard deviation [km/s]	0.3 – 0.5	
Moho input standard deviation [km]	0.75	

Table S3. PmP reflector inversion parameters for strong and weak regularization. If two values are present, the first one refers to line LI-02 and the second to line IS-01.

Parameter/Line	**strong Reg.**	**weak Reg.**
Reflector correlation length [km]	3	1.25
Reflector smoothing weight	50, 70	15
Reflector damping weight	50	10
χ^2_{pmp}	0.9, 1.0	0.5, 0.5